Dynamic voltage regulation using SVCs

A simulation study on the Swedish national grid

OSCAR SKOGLUND

KTH Electrical Engineering

Degree project in
Electric Power Systems
Second cycle
Stockholm, Sweden 2013

KTH Electrical Engineering

Dynamic voltage regulation using SVCs

A simulation study on the Swedish national grid

Oscar Skoglund
Stockholm, 2013

This masters thesis has been performed at:

Abstract

Voltage stability is a major concern when planning and operating electrical power systems. As demand for electric power increases, power systems are stressed more and more. The FACTS family of components were introduced to utilize the existing grid to a higher degree, while still maintaining system stability.

This thesis investigates if the addition of another SVC to the Swedish national grid could increase the power transfer from north to south. Placement of the SVC was based on two different indices used to indicate weak areas of the grid; the Q-V sensitivity index and the $VCPI$ index.

Simulations were performed with both the added SVC and regular switched shunt compensation and the results were compared against each other. Studies were also performed to investigate the effect of an SVC installed at the grid connection of a large (1000 MW) wind farm. Simulations were performed where the wind farm was modeled by either doubly fed induction generators (DFIG) or single cage induction generators.

This simulation study was performed using PSS$^{\text{TM}}$E, based on a detailed model of the Nordic power system as it existed in 2007.

The studies showed that adding a $\pm$200 MVAr SVC to the Swedish national grid could increase the power transfer by 150 MW, where an equally rated switched shunt capacitor/reactor would result in a 100 MW increase. In these studies, the transfer capacity was limited by voltage collapse situations.

However, installing the same $\pm$200 MVAr SVC at the connection of a large wind farm showed an increase in power transfer by 1000 MW, while the switched shunt compensation only resulted in a 500 MW increase. In the simulations that showed the greatest increase in transfer capacity, the added wind farm was modeled by single-cage induction generators. In this case the transfer capacity was limited by transient stability problems.

Contents

Abstract **i**

1 Introduction **2**
1.1 Background . . . 2
1.2 Literature review . . . 4
1.3 Thesis objectives . . . 4
1.4 Limitations . . . 4
1.5 Outline of this work . . . 5

2 Voltage stability **6**
2.1 Theoretical review . . . 7
2.1.1 Power flow on a short transmission line . . . 7
2.1.2 Maximum power transfer on a lossless transmission line . . . 9
2.1.3 Reactive power compensation to increase transfer of active power 10
2.2 Methods to assess voltage stability . . . 12
2.2.1 *P-V* curves . . . 13
2.2.2 *Q-V* curves . . . 15
2.2.3 *Q-V* sensitivity . . . 16
2.2.4 Voltage Collapse Proximity Indicator (VCPI) . . . 16
2.3 Forces of instability . . . 17
2.3.1 LTC transformers . . . 17
2.3.2 Stalling induction motors . . . 19

3 Static VAr Compensator (SVC) **20**
3.1 SVC components . . . 20
3.1.1 Thyristor switched capacitor . . . 21
3.1.2 Thyristor switched reactor . . . 23
3.1.3 Thyristor controlled reactor . . . 24
3.2 Common SVC topologies . . . 26
3.3 Control application and modelling . . . 26
3.3.1 Steady-state model . . . 27
3.3.2 Dynamic modelling . . . 27
3.4 Grid placement . . . 29

4 Case study **30**
4.1 Simulation methodology . . . 31
4.1.1 General simulation considerations . . . 31
4.1.2 Simulation considerations setting up a voltage collapse scenario . 32
4.2 Identification of suitable location for SVC installation . . . 32

4.2.1 Identification based on Q-V sensitivity . . . 33
4.2.2 Identification based on $VCPI$ . . . 33
4.3 Contingency identification . . . 35
4.4 Results from dynamic simulations . . . 36
4.4.1 Transfer limits of transmission interface SE2-SE3 . . . 36
4.4.2 A closer look at the voltage collapse . . . 38
4.4.3 Transfer capability with added SVCs . . . 41
4.4.4 Transfer capability with switched shunt compensation . . . 44
4.5 Wind power integration and voltage stability . . . 45
4.5.1 Wind farm modeled as squirrel cage induction generators . . . 45
4.5.2 Wind farm based on doubly fed induction generators (DFIGs) . . . 50
4.6 Study of the socio-economic benefits . . . 54

5 Conclusions and future work **56**
5.1 Conclusions . . . 56
5.2 Future work . . . 58

A Transfer data **60**

B List of calculated indices **62**
B.1 Q-V sensitivity . . . 62
B.2 $VCPI$ index . . . 63

C Wind model parameters **64**
C.1 CIMTR3 . . . 64
C.2 GE 3.6 MW, 50 Hz . . . 65

List of Figures

1.1 Overview of the Nordic power system. 3

2.1 One line diagram representing a short transmission line. 7
2.2 One line diagram representing the lossless transmission line. 9
2.3 Simple example system, one line and impedance load. 10
2.4 Example system with π modeled line and shunt capacitor. 12
2.5 Example of a P-V curve. 14
2.6 Nose curves shown for some different power factors. 14
2.7 Theoretical Q-V curves for two different levels of active power transfer. 15
2.8 Simple equivalent circuit of an LTC transformer. 17

3.1 One-line diagram of the common SVC components. 21
3.2 One-line diagram of a general TSC system. 23
3.3 $V - I$ characteristics of a TSC configuration using three capacitor branches. 23
3.4 TCR current for different values of α 25
3.5 $V - I$ characteristics of the TCR 25
3.6 SVC implemented in the load flow case as a variable shunt susceptance. 27
3.7 Block diagram representation of the IEEE basic model 1. 28
3.8 Block diagram of the voltage regulator used in the IEEE basic model 1. 28
3.9 Block diagram of the SVC model CSSCST 28

4.1 Swedish national grid marked with the current interfaces. 30
4.2 Example of a simulated Q-V curve, presented alongside its average slope. 34
4.3 $VCPI_Q$ of the investigated buses in the high transfer case. 35
4.4 Voltage profiles, bus 2 and contingency 6. 37
4.5 Voltage profiles different parts of Sweden, voltage collapse. 38
4.6 Voltage profiles of 6 buses in SE3, voltage collapse. 39
4.7 Voltage profiles, LTC operation and number of active limiters. 40
4.8 Voltage profiles and SVC response for 4 different SVC locations. 44
4.9 Voltage profiles bus 2, contingency 14, induction generator based wind farm. 46
4.10 Voltage level and reactive power exchange for wind farm. 47
4.11 Voltage profiles, LTC operation, active limiters for added wind farm. . . 48
4.12 $VCPI$ bar chart with a wind farm modeled as induction generators. . . 49
4.13 Voltage profiles, bus 2, contingency 14, induction generator based wind farm. 50
4.14 Voltage profiles, bus 2, reactive power of DFIG based wind farm. 52
4.15 $VCPI$ for studied buses with added DFIG based wind farm. 52
4.16 Electricity market benefit for the simulated scenarios. 55

List of Tables

4.1 The ten buses with the largest Q-V sensitivities. 34
4.2 List of the 10 buses with the highest $VCPI_Q$ values. 35
4.3 A list of the 15 contingencies that increase the SE2-SE3 transfer the most. 36
4.4 The five simulated cases and their level of transfer across SE2-SE3. . . . 37
4.5 CSSCST model parameters for two SVC configurations. 42
4.6 Suggested SVC buses with $VCPI$ and Q-V sensitivity rankings. 42
4.7 $N-1$ contingency for added SVC. 43
4.8 Results from the simulations for the different SVC placements. 43
4.9 Results from the simulations using switched shunts. 44
4.10 The simulated cases and their level of transfer across SE2-SE3. 45
4.11 $N-1$ contingency for the added wind farm. 46
4.12 $VCPI$ ranking for a case with an added wind farm. 49
4.13 Comparison of SVC and switched shunt compensation. 50
4.14 The simulated cases and their level of transfer across SE2-SE3. 51
4.15 $VCPI$ ranking for a case with an added DFIG based wind farm. 53
4.16 Results SVC and switched shunt for DFIG win farm. 53
4.17 Electricity market benefit for the different scenarios and interface increases. 54

5.1 Largest interface increase for different types of compensation. 56
5.2 Largest interface increase for different types of compensation. 57

A.1 Detailed transfer data for the different cases simulated. 60
A.2 Detailed transfer data for the different cases with added wind farm. . . 61
A.3 Transfer data for cases used in $VCPI$ calculations. 61

B.1 Q-V sensitivities for the investigated buses. 62
B.2 $VCPI_Q$ list for the investigated buses. 63

C.1 Load flow data for induction generator based wind farm. 64
C.2 List of the parameters used in the dynamic model CIMTR3. 64
C.3 Model: GECNA 65
C.4 Model: GEAERA 65
C.5 Turbine data 66
C.6 Model: GEDFA 66
C.7 Model: WGUSTA 66
C.8 Model: W2MSFA 67
C.9 Model: GEPCHA 67
C.10 Voltage and frequency protection parameters. 67

Nomenclature

List of acronyms

AC	Alternating Current
BID	Better Investment Decisions
DC	Direct Current
DFIG	Doubly Fed Induction Generator
FACTS	Flexible Alternating Current Transmission System
HVDC	High Voltage Direct Current
LTC	Load Tap Changing (transformer)
NTC	Net Transfer Capacity
OXL	Over-excitation Limiter
SSR	Sub Synchronous Resonance
SVC	Static Var Compensator
TCR	Thyristor Controlled Reactor
TSC	Thyristor Switched Capacitor
TSO	Transmission System Operator
TSR	Thyristor Switched Reactor
VCPI	Voltage Collapse Proximity Indicator
WTG	Wind Turbine Generator
PSS™E	Power System Simulator for Engineering

List of symbols

α	Thyristor firing angle	[rad]
B	Susceptance	[S]
$\cos\varphi$	Power factor	
C	Capacitance	[F]
I	Current	[A]
j	Imaginary number	
L	Inductance	[H]
ω_0	Nominal angular frequency	[rad/s]
φ	Phase angle between voltage and current	[rad]
P	Active power	[W]
Q	Reactive power	[VAr]
S	Apparent power	[VA]
θ	Bus voltage angle	[rad]
X	Reactance	[Ω]

Chapter 1

Introduction

Presenting a master thesis at the Royal Institute of Technology in Stockholm. The work has been performed at the Swedish transmission system operator, Svenska Kraftnät, in Sundbyberg, Sweden.

1.1 Background

Voltage stability is a major concern when planning and operating a modern power system. The last decade has seen a number of widespread blackouts in large power systems. Examples in recent times are [1–6]:

- The blackout in southern Sweden and eastern Denmark in September, 2003.
- The blackout in U.S. and Canada in August 2003.
- The blackout in Italy in September 2003.
- The blackout in Brazil and Paraguay 2009.
- The India blackout in July 2012.

These occurrences indicate that the subject of power system collapse still needs further investigation. One cause of system failure is voltage collapse, which will be studied throughout this thesis. The increasing power demand of the modern world contributes to the increased stress on the power system. Previously, the stress has been eased by adding more generation facilities to the grid and by building additional transmission lines.

Today it is much harder to acquire new rights of way to build new transmission lines in order to strengthen the grid. This calls for fresh approaches on how to utilise the existing grid more efficiently and to operate it closer to its thermal limit.

The introduction of the FACTS concept and components have led to new ways of increasing the stability limit of the existing power system. This is achieved by adding modern controllable components to the grid. An example of such a device is the SVC, which is the focus of this thesis.

Modern power systems are very complex, comprising thousands of generators, transmission lines and transformers. Here, we will concentrate on the Swedish national grid, which is part of the Nordic transmission network, which is shown in figure 1.1.

The aim of this work is to present the concept of voltage stability and to discuss how an SVC can affect the stability limits of the system based on its placement in the grid.

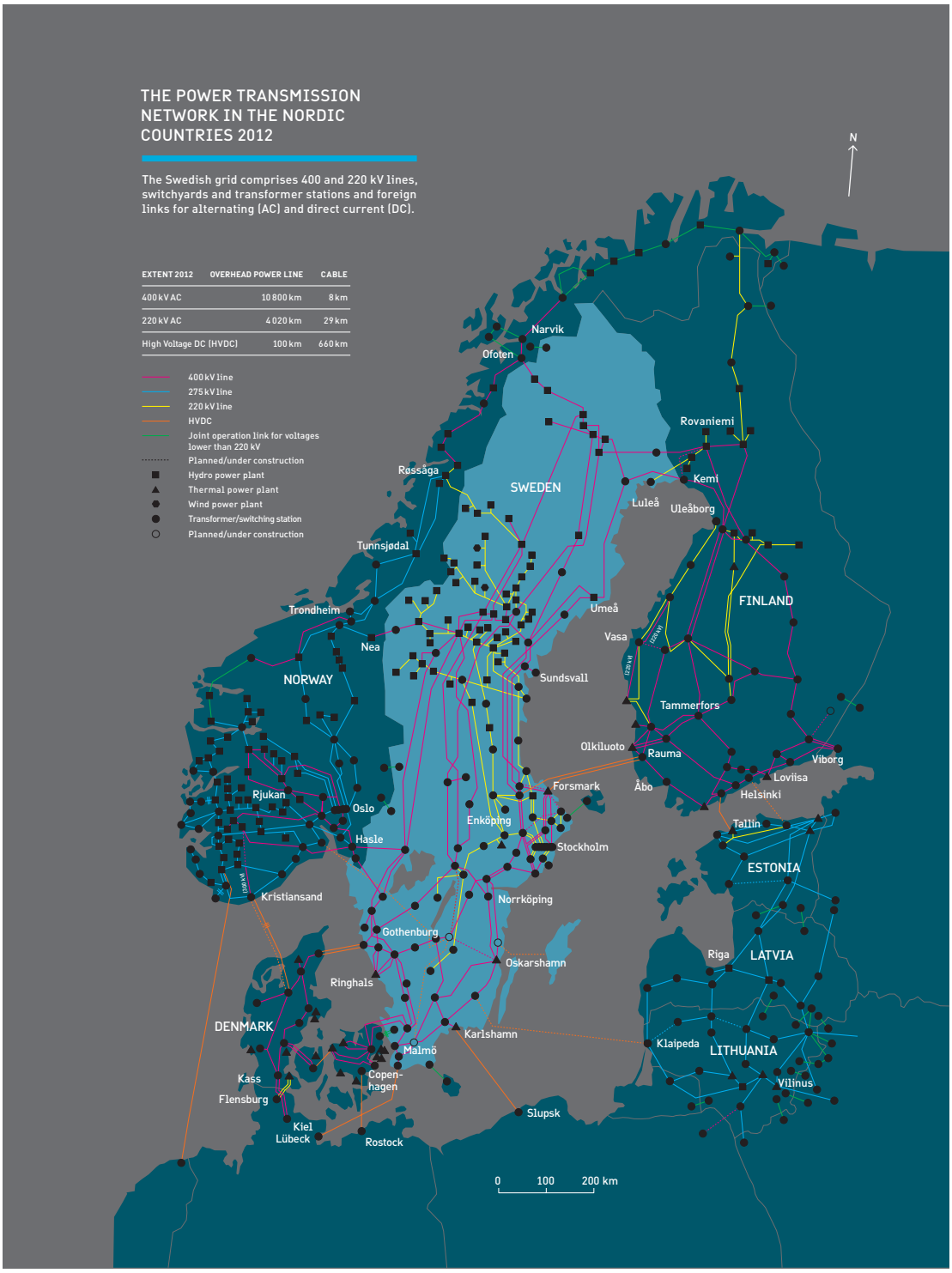

Figure 1.1: Overview of the Nordic power system.

1.2 Literature review

The concept of voltage stability has been thoroughly examined in various books and other publications the last few decades [7–10]. A wide range of analysis methods have been presented in order to investigate the conditions when a power system enters a state of unstable operation. Some of these methods include, e.g. P-V and Q-V curves and other methods based on eigenvalue analysis.

Reactive power compensation strategies have been developed in order to counteract power system instabilities [7, 8, 11]. Previously, these compensation strategies have been based on installing synchronous compensators, switched shunt compensation and series compensation.

The FACTS concept has introduced a number of new approaches and techniques to address power system stability [12]. One of the earliest components from the FACTS family is the SVC, introduced in the 1970s [13]. The SVC can be used in power systems to improve voltage control [14–16], improve transient stability [17], increase transmission capacity [18] and to improve power system damping [19].

Previous work has shown that the SVC should be placed at the weakest bus of the system to maximize its effect [20]. The weak buses can be identified by eigenvalue based modal analysis [21] or by using sensitivity analysis [22–24].

This work compares SVC placement based on Q-V sensitivity and the Voltage Collapse Proximity Indicator, $VCPI$ [20,25]. The two placement strategies are evaluated based on how the transmission capacity of a certain grid interface is improved.

The study is performed using a detailed model of the Nordic power system.

1.3 Thesis objectives

This thesis strives to answer the following questions:

- How should an SVC be placed in the grid to maximize its performance?
- Could the addition of SVCs improve the voltage stability margins of the Swedish national grid?
- Could the addition of SVCs increase power transfer capacity at a certain grid interface?
- What would be the socioeconomic impact of an increased power transfer capability?

1.4 Limitations

To narrow the scope of the thesis some limitations must be considered. The limitations of this work are as follows:

- All the simulations are performed using only the standard toolboxes in PSS™E 31.0.1. This means that it is not possible to perform eigenvalue analysis of the power system or optimal power flow analysis.
- Dynamic simulations are only based on existing SVC models.

1.5 Outline of this work

Chapter 1 introduces the work carried out in this thesis and lists its objectives and limitations.
Chapter 2 focuses on the concept of voltage stability.
Chapter 3 describes the operation of the SVC and how it could be used to increase grid stability.
Chapter 4 presents a simulation case study where additional compensation devices are installed in the Swedish grid such that their impact on grid performance may be examined. The simulation study have been performed using PSS^{TM}E.
Chapter 5 presents the conclusion and suggests future work within the studied area.

Chapter 2

Voltage stability

To ensure reliable operation, a power system has to be designed to withstand a large number of different disturbances. This is achieved by designing and operating the power system such that the most probable contingencies will not cause any loss of load, i.e. except at the direct connection to the equipment affected by the fault. It is especially important for the power system to be able to cope with the most severe contingencies without risking an uncontrolled spread of power interruptions (blackouts).

TSOs have a set of technical requirements which must be fulfilled throughout the entire power system. They apply from generation, via the transmission and distribution grids all the way to the connected loads (customers). One example of these requirements is limits on voltage level that applies to the terminals of all equipment in the system. The voltages have to be kept within an "acceptable limit" to protect both utility and customer equipment.

Keeping the voltages within predefined intervals is challenging by the fact that most power systems are quite complex. Loads connected to the system will vary over time, therefore the reactive power demand of the system will also vary. This will again lead to a variation of the voltage level as reactive power and voltage are closely coupled. Faults, disconnections and other contingencies also affect the demand of reactive power and voltage level in the system. It is crucial to keep a close eye on how the voltage level is varying throughout the power system and to make sure it is kept within the required limits. The goal is to have a power system that is "voltage stable".

Voltage stability is defined as the ability of a power system to maintain steady state voltages at all buses in the system after being subjected to a disturbance from a given initial operating condition [9].

A power system would thus be characterized as unstable if a disturbance led to an uncontrollable drop in voltage. This unstable event is termed as a "voltage collapse" or "voltage instability". The main cause of instability is the power system's lacking ability to meet the demand for reactive power [26]. Hence, problems with voltage instability most often occurs in heavily stressed power systems [8].

The aim of this chapter is to describe the concept of voltage stability in a power system and to present some analysis methods to investigate the system. This is done to give an insight into how the voltage stability margin of a power system can be extended.

2.1 Theoretical review

Throughout this thesis the term "load" is regarded as a portion of the system that is not explicitly represented in a system model. Rather, it is treated as if it was a single power-consuming device connected to a bus in the system model. Using this representation, the load will include, apart from the load itself, components like distribution transformers and feeders [27]. It makes sense to use this lumped model approach as we focus our studies on the Swedish national grid, i.e. the high voltage transmission system. Aggregating connected households together with the distribution grids and substations makes it possible to have a power system model with a reasonable level of complexity.

This section presents some basic theory regarding three phase power systems. It will explain the subject of power transfer and how it could be possible to increase the power transfer capacity of a transmission line. This theory is explained using a set of simple examples. These examples show the basic principles and they will form the basis for this thesis.

2.1.1 Power flow on a short transmission line

This section provides a simple example of how we can derive the power flow across a transmission line. We use a simple model to represent the transmission line as just an impedance connected between the sending and receiving buses. This approximation is considered valid for lines shorter than about 80 km [8].

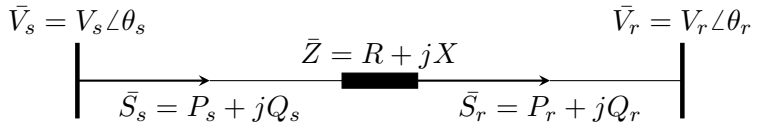

Figure 2.1: One line diagram representing a short transmission line.

We base this derivation on the simple system shown in figure 2.1. The sending end is represented by the bus voltage $\bar{V}_s$ and the receiving end by $\bar{V}_r$. The two buses are connected via a line, represented by the impedance $\bar{Z}$. We can now describe the apparent power injected to the line as

$$\bar{S}_s = \bar{V}_s\bar{I}^* = \bar{V}_s\left(\frac{\bar{V}_s^* - \bar{V}_r^*}{\bar{Z}^*}\right) = \frac{\bar{V}_s^2}{\bar{Z}^*} - \frac{\bar{V}_s\bar{V}_r^*}{\bar{Z}^*} = \frac{\bar{V}_s^2}{R - jX} - \frac{|\bar{V}_s||\bar{V}_r|}{R - jX}e^{j(\theta_s - \theta_r)} \tag{2.1}$$

which can be rewritten as

$$\bar{S}_s = \frac{\bar{V}_s^2}{Z^2}(R + jX) - \frac{|\bar{V}_s||\bar{V}_r|}{Z^2}(R + jX)\left(\cos(\theta_s - \theta_r) + j\sin(\theta_s - \theta_r)\right) \tag{2.2}$$

where Z is the absolute value of the impedance $R + jX$. Splitting (2.2) into its real and imaginary parts gives us the expressions for the active and reactive powers injected to the line:

$$P_s = \frac{V_s^2}{Z^2}R - \frac{V_sV_r}{Z^2}\left(R\cos(\theta_s - \theta_r) - X\sin(\theta_s - \theta_r)\right) \tag{2.3}$$

$$Q_s = \frac{V_s^2}{Z^2}X - \frac{V_sV_r}{Z^2}\left(R\sin(\theta_s - \theta_r) + X\cos(\theta_s - \theta_r)\right) \tag{2.4}$$

Correspondingly, the active and reactive powers fed to the receiving end become:

$$P_r = -\frac{V_r^2}{Z^2}R + \frac{V_s V_r}{Z^2}\left(R\cos(\theta_s - \theta_r) + X\sin(\theta_s - \theta_r)\right) \tag{2.5}$$

$$Q_r = -\frac{V_r^2}{Z^2}X - \frac{V_s V_r}{Z^2}\left(R\sin(\theta_s - \theta_r) - X\cos(\theta_s - \theta_r)\right) \tag{2.6}$$

In high voltage overhead lines, the reactance is usually the dominating part, i.e. $R << X$. Neglecting the resistance gives us this approximation of the active power flow equations (2.3) and (2.5):

$$P_s \approx P_r \approx \frac{V_s V_r}{X}\sin(\theta_s - \theta_r) \tag{2.7}$$

Hence, the direction of the active power flow is determined by the phase angles θ_s and θ_r. In almost every case the active power flows "toward the lower angle".

If we now assume that the voltages at the sending and receiving buses are almost in phase ($\theta_s - \theta_r \approx 0°, \cos(\theta_s - \theta_r) \approx 1$). If we also neglect the resistance in (2.4) and (2.6), we can approximate the reactive power flow equations as:

$$Q_s = \frac{V_s(V_s - V_r)}{X} \tag{2.8}$$

$$Q_r = \frac{V_r(V_s - V_r)}{X} \tag{2.9}$$

Based on the approximations (2.8) and (2.9) it becomes clear that reactive power flow is mainly dependent on voltage magnitudes. The power flows from the highest voltage to the lowest voltage [7]. Two useful rules of thumb are

- active power and power angles are closely coupled
- reactive power and voltage magnitude are closely coupled.

If we now shift focus and concentrate on the active and reactive losses in a power system. Losses across the transmission line, modeled by the impedance Z, are determined by

$$P_{loss} = RI^2 \tag{2.10}$$

$$Q_{loss} = XI^2 \tag{2.11}$$

where I^2 can be rewritten as

$$I^2 = \bar{I}\bar{I}^* = \left(\frac{P + jQ}{\bar{V}}\right)\left(\frac{P - jQ}{\bar{V}^*}\right) = \frac{P^2 + Q^2}{V^2} \tag{2.12}$$

We can now rewrite the loss expressions (2.10) and (2.11) as:

$$P_{loss} = R\frac{P^2 + Q^2}{V^2} \tag{2.13}$$

$$Q_{loss} = X\frac{P^2 + Q^2}{V^2} \tag{2.14}$$

If we study (2.13) and (2.14), we notice that the losses in a power system can be minimized by transferring power at as high voltages as possible. We also notice that the losses are proportional to S^2 and that transferring reactive power, Q, will increase the active power loss.

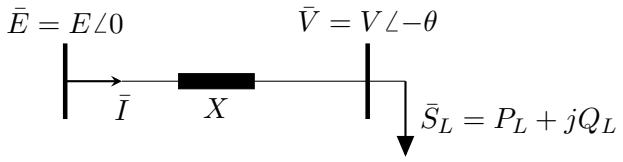

Figure 2.2: One line diagram representing the lossless transmission line.

2.1.2 Maximum power transfer on a lossless transmission line

In this example [26] we consider the very simple system in figure 2.2 which comprises an ideal voltage source $\bar{E} = E\angle 0$ feeding a load at voltage $\bar{V} = V\angle -\theta$ through a lossless line represented by its reactance X. Balanced three-phase operation is assumed.
The voltage $\bar{V}$ at the load bus is determined by

$$\bar{V} = \bar{E} - jX\bar{I} \tag{2.15}$$

where the voltage magnitude and phase angle have been reduced across the line reactance X. The apparent power, $\bar{S}_L$, absorbed by the load is defined as

$$\bar{S}_L = P_L + jQ_L = \bar{V}\bar{I}^* = -\frac{EV}{X}\sin\theta + j\left(-\frac{V^2}{X} + \frac{EV}{X}\cos\theta\right) \tag{2.16}$$

and can be rearranged as the familiar power flow equations:

$$P_L = -\frac{EV}{X}\sin\theta \tag{2.17}$$

$$Q_L = -\frac{V^2}{X} + \frac{EV}{X}\cos\theta \tag{2.18}$$

Using the trigonometric identity to eliminate θ from (2.16) yields:

$$(V^2)^2 + (2Q_LX - E^2)V^2 + X^2(P_L^2 + Q_L^2) = 0 \tag{2.19}$$

The second-order expression with respect to V^2 in (2.19) have the following solutions:

$$V^2 = -\frac{2Q_LX - E^2}{2} \pm \sqrt{(2Q_LX - E^2)^2 - 4X^2(P_L^2 + Q_L^2)} \tag{2.20}$$

To ensure the existence of a real solution, the square root in (2.20) must fulfill

$$(2Q_LX - E^2)^2 - 4X^2(P_L^2 + Q_L^2) \geq 0 \tag{2.21}$$

which can be expanded as

$$-4X^2P_L^2 - 4Q_LXE^2 + E^4 \geq 0 \tag{2.22}$$

and rewritten as:

$$-P_L^2 - \frac{E^2}{X}Q_L + \left(\frac{E^2}{2X}\right)^2 \geq 0 \tag{2.23}$$

If we assume that only reactive power is transferred across the line ($P = 0$ in (2.23)), the maximum reactive power that can be delivered to the load is:

$$Q_L \leq \frac{E^2}{4X} \tag{2.24}$$

We do the corresponding assumption for a completely active power transfer ($Q = 0$ in (2.23)). In this case, the maximum active power that can be delivered to the load is:

$$P_L \leq \frac{E^2}{2X} \tag{2.25}$$

In an electrical power system, the highest possible power transfer that can occur is defined as the short-circuit power. The short-circuit power is determined by the system voltage level and system impedance. This power transfer would only occur following a fault and does not represent a viable mode of operation. In our example system, the short-circuit power at the load bus is defined as:

$$S_{sc} = \frac{E^2}{X} \tag{2.26}$$

This may be compared to the maximum delivery of reactive and active power in (2.24) and (2.25). The maximum active power transfer is half the size of the short-circuit power, while its reactive counterpart is only a quarter of the size.

Therefore we may conclude that it is not "as easy" to transfer large amounts of reactive power over long transmission lines compared to active power transmission. This is due to the inductive nature of an electrical power system and this example shows why we may benefit from supplying additional reactive power to the grid. If reactive power could be injected closer to the major load centers it would reduce the stress on the transmission lines. This was also indicated earlier in section 2.1.1 by discussing how transfer of reactive power increases transmission line losses.

2.1.3 Reactive power compensation to increase transfer of active power

As was shown in section 2.1.2, reactive power proves difficult to transfer in a power system. Section 2.1.1 illustrated that transferring reactive power will also increase the losses in the system. Thus, it would be desirable to produce reactive power as close to the loads as possible. Reducing losses by additional production of reactive power should enable us to increase the transfer of active power.

One way to add reactive power production is to install shunt connected capacitors to the grid. A shunt capacitor produces reactive power as described by

$$Q_{sh} = B_{sh}V^2 \tag{2.27}$$

where B_{sh} is the capacitor susceptance and V is the applied capacitor voltage.

To describe how the addition of a shunt connected capacitor would affect the transfer of power, we study another example. Consider the very simple, general example system shown in figure 2.3 below.

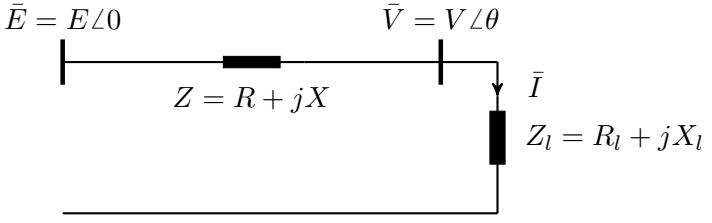

Figure 2.3: Simple example system represented by an ideal voltage source, a transmission line and a connected impedance load.

In this system, the load Z_l is fed by the ideal voltage source E, via the transmission line described by Z. The current through the example system is determined by

$$\bar{I} = \frac{\bar{E}}{(R + R_l) + j(X + X_l)} \tag{2.28}$$

where the active power delivered to the load is determined by:

$$P = R_l I^2 = \frac{R_l E^2}{(R + R_l)^2 + (X + X_l)^2} \tag{2.29}$$

If we assume the load power factor to be $\cos\varphi$ we can describe the load impedance using only one unknown quantity:

$$Z_l = R_l + jX_l = R_l + jR_l \tan\varphi \tag{2.30}$$

We can now use (2.30) to rewrite the system current as

$$\bar{I} = \frac{\bar{E}}{(R + R_l) + j(X + R_l \tan\varphi)} \tag{2.31}$$

and the delivered active power as

$$P = R_l I^2 = \frac{R_l E^2}{(R + R_l)^2 + (X + R_l \tan\varphi)^2} \tag{2.32}$$

If we now consider the case with a lossless transmission line, i.e. $R = 0$, we can determine the maximum transfer of active power under a constant power factor. If we connect the load R_{lmaxP} as described by [26]

$$R_{lmaxP} = X \cos\varphi \tag{2.33}$$

we will maximize the active power transfer under the constant power factor $\cos\varphi$.

Inserting (2.33) into (2.32), we get the following expression describing the maximum transfer of active power.

$$P_{max} = \frac{X \cos\varphi E^2}{(X \cos\varphi)^2 + (X + X \cos\varphi \tan\varphi)^2} = \frac{\cos\varphi}{1 + \sin\varphi} \frac{E^2}{2X} \tag{2.34}$$

The corresponding load bus voltage is determined by [26]:

$$V_{maxP} = \frac{E}{\sqrt{2}\sqrt{1 + \sin\varphi}} \tag{2.35}$$

In the studied example systems, shown in figures 2.2 and 2.3, the transmission lines have been modeled by a single impedance. We now extend the model by describing the transmission line using the "π model"[†] and adding a shunt connected capacitor. The result is the compensated example system in figure 2.4 below.

In figure 2.4, the susceptance B_l describes the line-to-ground capacitance of the line and B_c is the shunt capacitor susceptance. P and Q describes the active and reactive power delivered to the load.

[†]The π model of a transmission line refers to when the line model is expanded by modeling the line-to-ground capacitance. Adding the capacitors will make the line model look like the greek letter π.

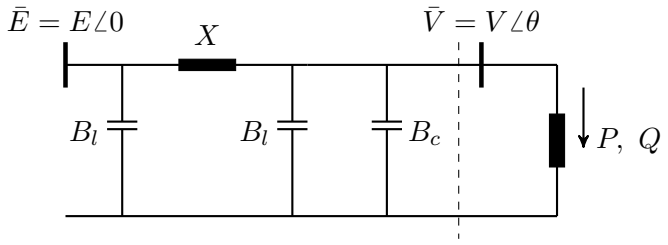

Figure 2.4: An example system where the transmission line is described using the π model and a shunt capacitor is added to inject reactive power.

We make a Thévenin equivalent of the grid as seen by the load (lumping together everything left of the dashed line in figure 2.4). The Thévenin equivalent voltage and reactance are described by:

$$E_{th} = \frac{1}{1-(B_c+B_l)X}E \tag{2.36}$$

$$X_{th} = \frac{1}{1-(B_c+B_l)X}X \tag{2.37}$$

If we insert (2.36) and (2.37) into (2.34) and (2.35), we end up with:

$$P_{max} = \frac{\cos\varphi}{1+\sin\varphi}\frac{E_{th}^2}{2X_{th}} = \frac{1}{1-(B_c+B_l)X}\frac{\cos\varphi}{1+\sin\varphi}\frac{E^2}{2X} \tag{2.38}$$

$$V_{maxP} = \frac{E_{th}}{\sqrt{2}\sqrt{1+\sin\varphi}} = \frac{1}{1-(B_c+B_l)X}\frac{E}{\sqrt{2}\sqrt{1+\sin\varphi}} \tag{2.39}$$

Comparing (2.38)–(2.39) to (2.34)–(2.35), we note that both the delivered power and load bus voltage level have increased by the same factor. Inserting additional reactive power will thus increase the maximum power transfer. It will, however, also increase the voltage level of the load bus. This voltage increase can cause problems and it has to be monitored and considered when designing and operating the grid.

2.2 Methods to assess voltage stability

Planning and operating an electrical power system require that the planner/operator is constantly considering the various grid limitations. Limitations on individual components, i.e. transmission lines, transformers and other grid connected equipment are determined by the rating of the equipment. These limitations are straight forward to assess as the constraints are, e.g. temperature and current, two physical quantities that are quite easy to measure and monitor in a modern power system.

Voltage instability on the other hand is a phenomena that is dependent on the operating state of the whole power system. To identify a possible collapse situation, a system wide approach is needed. This section aims to answer how voltage instability can be predicted by some well recognized analysis methods.

2.2.1 P-V curves

P-V curves or "nose curves" can be used to illustrate the basic phenomena associated with voltage instability [8]. These curves are obtained by plotting the active power transfer P across a grid interface versus the voltage V at a representative bus. By increasing the interface transfer, the voltage of the studied bus will begin to drop as the grid is stressed more and more. Eventually the power transfer will reach its maximum and the voltage now drops rapidly as the load demand continues to increase. The power-flow solutions will not converge beyond this point, indicating system instability.

Knowing the point of instability makes it possible to determine the stability margin of the grid at a certain operating point. These curves are commonly used by grid operators to guarantee that a sufficiently large margin is kept to accommodate for contingencies.

We now shift focus to how these curves are defined and how different grid parameters affects the transmission capacity. P-V curves are defined by (2.20), previously derived in section 2.1.2. If we assume that condition (2.23) holds, the solution to (2.20) is given by

$$V = \sqrt{\frac{E^2}{2} - QX \pm \sqrt{\frac{E^4}{4} - X^2P^2 - XE^2Q}} \tag{2.40}$$

where we assume that the power factor is kept constant and the load is fed by the constant voltage E through a constant admittance X. By keeping the power factor constant, the reactive power can be rewritten as a function of active power and phase angle:

$$Q = P\tan\varphi \tag{2.41}$$

Inserting (2.41) into (2.40) gives us the load bus voltage as a function of active power:

$$V = \sqrt{\frac{E^2}{2} - P\tan\varphi X \pm \sqrt{\frac{E^4}{4} - X^2P^2 - XE^2P\tan\varphi}} \tag{2.42}$$

We set $E = 1.0$ p.u., $X = 1.0$ p.u., $\cos\varphi = 1.0$ and plot the load bus voltage V versus transferred active power P. Doing so we will end up with the P-V curve shown in figure 2.5. At a constant power factor, active power can be transferred at two different voltage levels, a higher and a lower as seen in figure 2.5. Power transfer at the lower voltage level leads to a higher current. As a real transmission system have losses, a larger current will lead to higher losses. This will translate to higher costs for power distribution companies and a higher wear on e.g. transformers. Only the upper operating point is considered a satisfactory operating point [8]. At the tip of the curve there is only one operating point which corresponds to the maximal power transmission P_{max}.

In section 2.1.2 we could see that the maximal transfer of active power through a lossless transmission line is described by (2.25). A lossless line represented by $X = 1.0$ p.u. fed by the stiff voltage source $E = 1.0$ p.u. can transfer the maximal active power $P_{max} = 0.5$ p.u.

P-V curves can also be used to visualize how the transfer capacity of the grid is affected by changing some parameters in the grid. In section 2.1.3 we could see that adding reactive power would affect both active power transfer and voltage level. Adding shunt compensation to the load bus will effectively alter the power factor. If the voltage level V of the load bus is plotted as a function of active power at different constant power factors, we will obtain the P-V curves shown in figure 2.6. Figure 2.6 clearly illustrates how altering the power factor will affect voltage level and maximum power transfer.

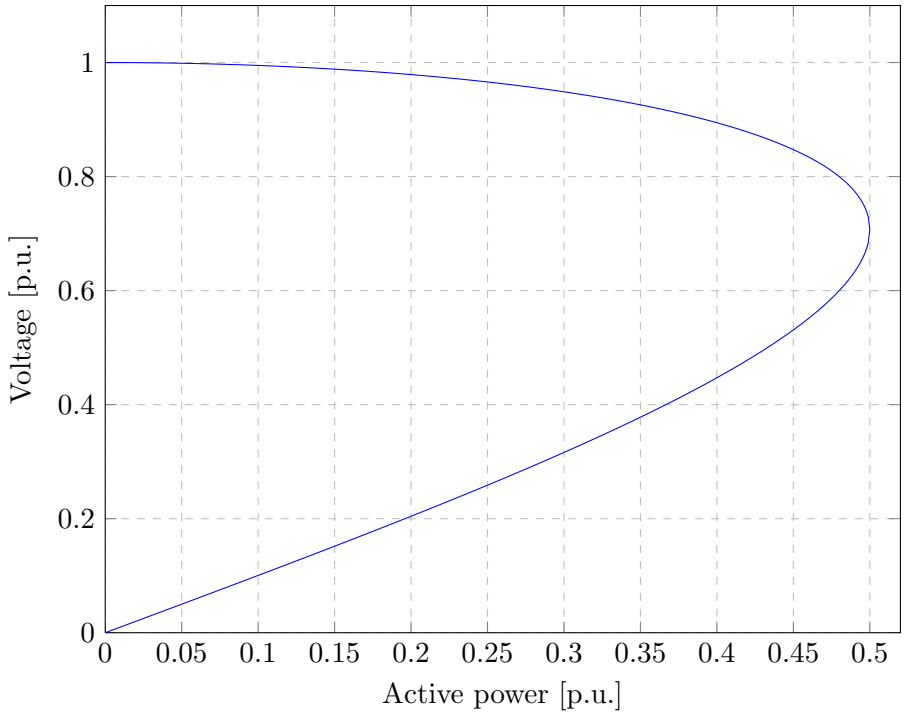

Figure 2.5: Example of a P-V curve.

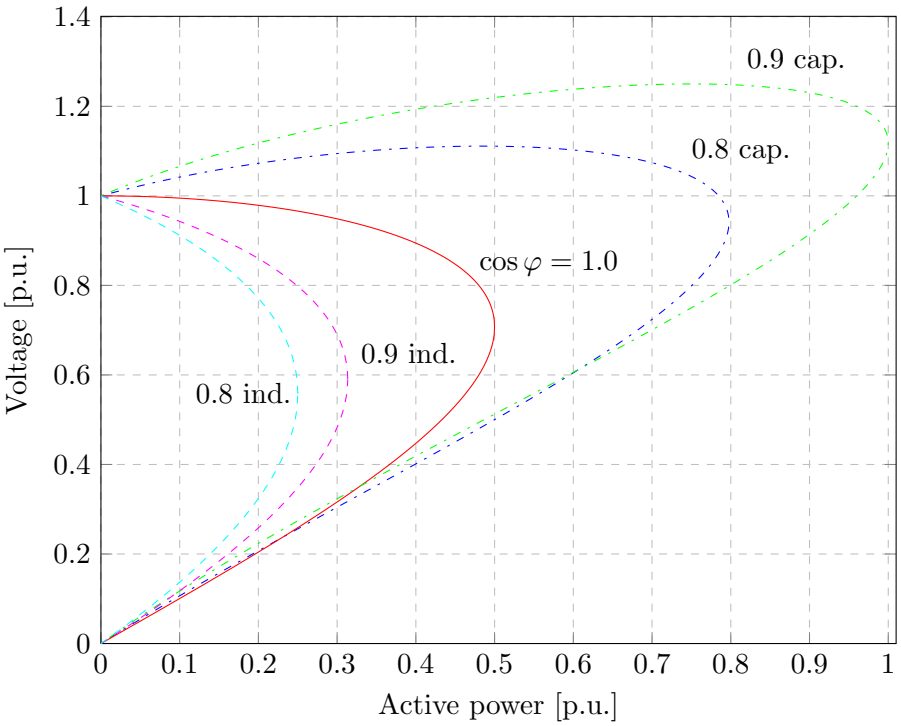

Figure 2.6: Nose curves shown for some different power factors.

2.2.2 Q-V curves

P-V curves can be used to illustrate how the active power transfer affects the load bus voltage. To get a clearer picture, we can introduce the concept of Q-V curves. For a chosen study bus, these curves can be used to illustrate the relationship between reactive power and voltage for a fixed value of active power transfer. Note that this section only provides a brief summary of the general theory regarding how these curves can be acquired.

We can obtain these curves by a number of power flow calculations [7]. First, a fictitious synchronous condenser[‡] is connected to a bus which is to be studied. Note that this fictitious condenser is set to have no reactive power limits. Then we run a series of power flow simulations where we vary the scheduled voltage of the synchronous condenser and note the associated reactive power production for each voltage level. If we now plot the reactive power versus the voltage, we will end up with a plot similar to the curves shown in figure 2.7.

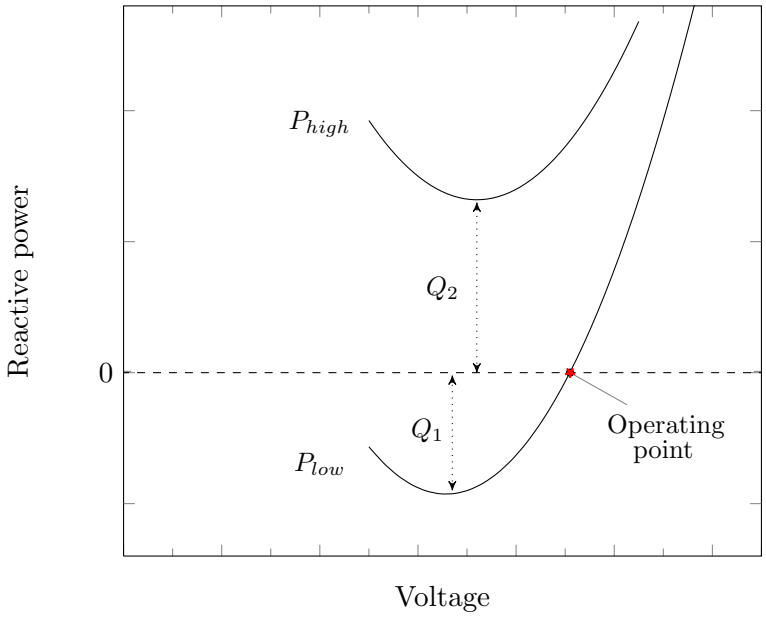

Figure 2.7: Theoretical Q-V curves for two different levels of active power transfer.

These curves can tell us something about the stability of the studied power system. A power system is considered stable in the region where the gradient of the Q-V curve is positive, i.e. the voltage level will increase if reactive power is injected. The Q-V curve minimum represents the voltage stability limit (the critical operating point of the system). Hence, the power system is considered stable to the right hand side of the minimum and unstable to the left hand side [8].

We can also use the simulated curves to evaluate the reactive power margin at the studied bus. Figure 2.7 shows two Q-V curves representing two different transfers of active power, P_{low} and P_{high}. In the lower transfer case we note the intersection between the Q-V curve and the dashed line corresponding to zero reactive power exchange between our fictitious condenser and the grid. This intersection point represents the current operating point of the studied system.

[‡]A synchronous condenser is a synchronous generator with no active power production. By varying the magnetization of the machine, it can be controlled to consume or generate reactive power.

If we now focus on the margin between the minimum of the lower curve and the dashed line in figure 2.7. This margin (Q_1) represents the reactive power margin of this operating point at the studied bus, i.e. we can add an additional reactive power load equal to Q_1 without losing stability.

Looking at the upper case with a higher power transfer we can see that there is no intersection with the dashed zero line. Hence, there is no operating point and this case is an unstable case. Here we note that the margin (Q_2) is located above the zero line, i.e. we need to add an additional Q_2 of reactive power to the studied bus to get a viable operating point.

In these curves we can clearly see how increasing the transfer of active power will affect the reactive power demand.

2.2.3 Q-V sensitivity

One way to identify areas in the grid prone to a voltage collapse is to calculate the Q-V sensitivity at selected buses [8, 28]. The Q-V sensitivity represents the slope of the $\Delta Q/\Delta V$ curve at the selected bus at a given operating point. As the voltage level of the bus is heavily dependent on its reactive power injection, the Q-V sensitivity is a measure of the bus' "stiffness" [7].

A positive slope represents stable operation, i.e. the bus voltage increases when the reactive power injection is increased. The smaller the gradient of the positive slope, the less sensitive the system will be. As the sensitivity index (slope of the Q-V curve), increases toward an infinite value, the system enters a state of instability. Therefore, the weaker buses can be identified by determining which have the steepest positive slopes.

2.2.4 Voltage Collapse Proximity Indicator (VCPI)

Another way to identify weak buses suggested in the literature is the Voltage Collapse Proximity Indicator ($VCPI$) [7, 20, 25]. This index varies from close to (but greater than) unity at a situation of low load to infinity at a collapse situation. The $VCPI$ can be used to determine the most effective locations for emergency load shedding and/or used for finding the buses which are located most effectively for reactive power compensation. As we are interested in locations for reactive power compensation, we will calculate the index which relates to reactive power – $VCPI_Q$.

$VCPI_Q$ relates how the total generation of reactive power in the system is affected by an increase in reactive power load at bus i. The $VCPI$ with respect to reactive power at the studied bus, i, is defined as [25]:

$$VCPI_{Q_i} = \frac{\sum\limits_{j \in \Omega_G} \Delta Q_{g_j}}{\Delta Q_i}, \qquad i \in \Omega_L \tag{2.43}$$

where Ω_G and Ω_L are sets of the generator buses and the studied load buses respectively. ΔQ_i represents a small increase in reactive power demand at the studied bus i and ΔQ_{g_j} is the increase in reactive power generation of generator j.

The weakest bus of the studied grid is determined by identifying the bus with the highest $VCPI_Q$ value. Bus k will thus be the weakest bus if the following holds:

$$VCPI_{Q_k} = \max_{i \in \Omega_L} \{VCPI_{Q_i}\} \tag{2.44}$$

It should be noted that the $VCPI$ is used to identify the weak buses of the current operating point of the studied system.

2.3 Forces of instability

In this section we discuss some grid mechanisms that could lead the system into a state of voltage instability. These forces are not usually instability mechanisms by themselves, but in heavily stressed power systems they could act as a catalyst for voltage instability.

We will focus our discussion on how the LTC transformers affect voltage stability and also mention the effects of stalling induction motors.

2.3.1 LTC transformers

Load tap changing (LTC) transformers are commonly used in modern power transmission systems to add an additional level of control. These transformers have the ability to adjust their turn ratio without interrupting the power flow through the apparatus. By changing the turn ratio, they can be used to control voltage and reactive power flow in the grid. Usually, the variable taps are located on the high voltage side of the transformer. This enables control of the lower voltage level to attempt to hold constant voltage at the point of consumption. Thus, voltage control capability of the LTC transformers plays an important role in load restoration following a disturbance in the grid.

We can find these transformers in different places of the grid and depending on the system they can be installed as either [26]:

- transformers feeding the distribution systems
- transformers connecting sub-transmission and transmission systems
- transformers connecting two transmission levels
- generator step-up transformers.

In the Swedish transmission system, LTC transformers are installed between the transmission system (at 400 and 220 kV) and the sub-transmission system (at 135 and 77 kV). They are also installed between the sub-transmission system and the distribution power system.

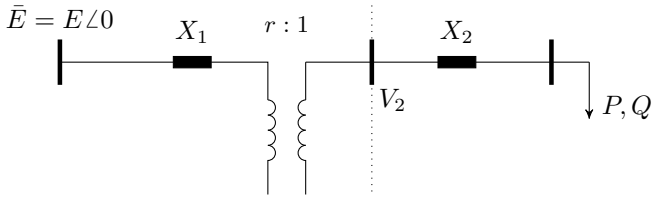

Figure 2.8: Simple equivalent circuit of an LTC transformer.

To understand how LTC transformers are used in power systems, we introduce the simple equivalent circuit shown in figure 2.8. In this circuit, the primary side reactance X_1 represents the equivalent reactance of the transmission system. This holds true if we assume the studied transformer is connected between, e.g. the sub-transmission and the transmission system. Similarly, the secondary side reactance X_2 represents the reactance of the sub-transmission and transmission systems. For simplicity, we assume the transformer to be ideal and include the leakage reactance in X_2.

The Thévenin equivalent seen by the load is represented by the following emf

$$E_{th} = \frac{E}{r} \tag{2.45}$$

and corresponding reactance

$$X_{th} = \frac{X_1}{r} + X_2 \tag{2.46}$$

where r is the tap ratio of the LTC transformer.

If we insert (2.45) and (2.46) into (2.34) and (2.35), we can determine how LTCs affect the maximum deliverable power (at the constant $\cos\varphi$). Described by

$$P_{max} = \frac{1}{2}\ \frac{\cos\varphi}{1+\sin\varphi}\ \frac{E^2}{r^2 X_2 + X_1} \tag{2.47}$$

and the corresponding voltage:

$$V_{maxP} = \frac{E}{r\sqrt{2}\sqrt{1+\sin\varphi}} \tag{2.48}$$

In normal operating conditions, r is decreased to achieve an increase in voltage V_2. Increasing r will correspondingly decrease the voltage. We can see in (2.47) that decreasing r will also increase the maximum deliverable power to the load.

The variable tap of the LTC is limited by the number of windings on the controllable side of the transformer. This will put a constraint on the LTC tap ratio r described by:

$$r_{min} \leq r \leq r_{max} \tag{2.49}$$

Typical values of r_{min} are 0.85–0.90 p.u. and for r_{max} in the range 1.10–1.15 p.u. The size of each step is usually between 0.5%–1.5% [26].

We now consider an example [8] where a fictitious power system is in a very stressed state and a number of key transmission lines are heavily loaded. Following a disturbance, one of these lines is disconnected, which further increase the loading of the remaining lines. This will cause the reactive power demand of the system to increase even further due to the increased reactive power losses in the lines.

Losing this heavily loaded transmission line will cause a voltage drop at nearby load centers. To counteract this drop in voltage, LTC transformers in the area will attempt to restore voltage and loads in the distribution grid. Each change in tap ratio to restore loads will increase the stress in the transmission lines. This will cause an increase of both active power losses, P_{loss}, and reactive power losses, Q_{loss}, in the high voltage transmission system. In very heavily loaded lines, each additional MVA transferred will cause several MVArs of line losses [8]. These additional losses will further decrease the voltage level of the transmission system.

To compensate for the higher reactive power demand in the system, the reactive power output of the connected generators have to increase. Eventually, the generators would hit their reactive power limit governed by the overexcitation limiters and cause its terminal voltage to drop. As this cause of event spreads amongst the generators, this process will eventually lead up to a voltage collapse situation.

The driving force behind this voltage collapse situation is the load restoration performed by the LTC transformers. Restoring the loads will increase the stress on the transmission system by increasing the reactive power consumption. Hence, causing the voltage level to reduce further [9].

2.3.2 Stalling induction motors

Induction motors make up a large portion of the total system load and is the workhorse of the electric industry. It is therefore important to be familiar with how induction motors affects voltage stability. We will use this section to briefly discuss how induction motors may influence a voltage collapse scenario.

At low voltages, typically below 0.9 or 0.85 p.u. [7, 8], some induction motors might stall and draw a large reactive current. Stalling of one motor might cause nearby motors to stall as well. The increased demand of reactive power caused by the stalling motors will affect the voltage level of the nearby power system. In a worst case scenario this could cause a voltage collapse.

Large industrial motors have protection systems to disconnect the motors from the power system in case of low voltage. After some time, the motors are reconnected and if the original cause of voltage problem still persists, the voltage will begin to drop again.

Small motors are usually not equipped with undervoltage protection but only have a thermal overload protection. Some examples may be refrigerators, single-phase air conditioners and household appliances. These motors might be stalled for several seconds before the thermal protection disconnects them. During this time, the motors will draw a reactive current up to four to six times normal, prolonging the voltage dip.

Chapter 3

Static VAr Compensator (SVC)

The Static VAr Compensator (SVC) is today considered a very mature technology. It has been used for reactive power compensation since the 1970s [13, 29, 30]. There are multiple applications within power systems, e.g. to increase power transfers across limited interfaces, to dampen power oscillations and to improve the voltage stability margins.

An SVC is a shunt connected FACTS device whose output can be adjusted to exchange either capacitive or inductive currents to the connected system. This current is controlled to regulate specific parameters of the electrical power system (typically bus voltage) [31].

The thyristor has been an integral part in realizing the SVC and to enable control of its reactive power flow. It is used either as a switch or as a continuously controlled valve by controlling the firing angle [32]. It should be noted that the SVC current will contain some harmonic content, something that needs attention in the design process.

The SVC can be used to control the voltage level at a specific bus with the possibility of adding additional damping control. This can effectively dampen oscillations in the power system such as sub synchronous resonances (SSR), inter-area oscillations and power oscillations.

SVCs are used at a large number of installations around the world and is still considered an attractive component to improve the performance of AC power systems. Examples of modern SVC installations can be found in e.g. Finland and Norway. These installations were commissioned to dampen inter-area oscillations and to enable a power transfer increase across a limited interface [33, 34].

The purpose of this chapter is to give a general review of how an SVC works, from specific components to general control strategies.

A description of the different possible "building blocks" of an SVC is presented in the section which here follows. Section 3.2 presents common SVC topologies, section 3.3 presents general control strategies and section 3.4 presents placement strategies to maximize the benefit of an SVC installation.

3.1 SVC components

This section presents the different "building blocks" that are commonly used when designing an SVC. The components are presented individually to describe their influence on the grid. We will also briefly discuss some of the problems associated with the

components and how these could be handled. This is done to give some insight into how an SVC operates.

The different building blocks presented in this section are illustrated in figure 3.1.

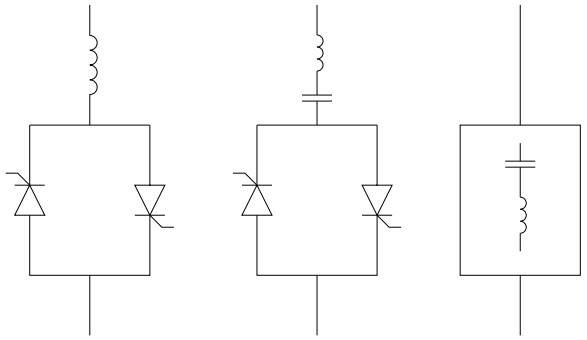

(a) TCR / TSR **(b)** TSC **(c)** Filter

Figure 3.1: One-line diagram of the common SVC components.

3.1.1 Thyristor switched capacitor

The thyristor switched capacitor (TSC), first introduced by ASEA in 1971, is a shunt connected capacitor that is switched ON or OFF using thyristor valves [31]. Figure 3.1(b) shows the one-line diagram of this component. The reactor connected in series with the capacitor is a small inductance used to limit currents. This is done to limit the effects of switching the capacitance at a non-ideal time [35].

We assume that the TSC in figure 3.1(b) comprises the capacitance C, the inductance L and that a sinusoidal voltage is applied

$$v(t) = V\sin(\omega_0 t) \tag{3.1}$$

where ω_0 is the nominal angular frequency of the system, i.e. $\omega_0 = 2\pi f_0 = 2\pi 50$ rad/s in a 50 Hz system.

The current through the TSC branch at any given time is determined by [36]

$$i(t) = \underbrace{I\cos(\omega_0 t + \alpha)}_{Steady-state} \underbrace{- I\cos(\alpha)\cos(\omega_r t) + nB_c\left(V_{C0} - \frac{n^2}{n^2-1}V\sin(\alpha)\right)\sin(\omega_r t)}_{Oscillatory\ transients} \tag{3.2}$$

where α is the thyristor firing angle, ω_r is the TSC resonant frequency, V_{C0} is the voltage across the capacitor at $t = 0$. The current amplitude I is determined by

$$I = V\frac{B_C B_L}{B_C + B_L} \tag{3.3}$$

where B_C is the capacitor susceptance and B_L is the reactor susceptance and n is given by:

$$n = \frac{1}{\sqrt{\omega_0^2 LC}} = \sqrt{\frac{X_C}{X_L}} \tag{3.4}$$

X_C and X_L above are the reactances of the capacitor and reactor. The TSC resonant frequency, ω_r, is defined by

$$\omega_r = n\omega_0 = \frac{1}{\sqrt{LC}} \tag{3.5}$$

We can alternatively express the magnitude of the TSC current (3.3), as [35, 36]

$$I = V\frac{B_C B_L}{B_C + B_L} = VB_C\frac{n^2}{n^2 - 1} \tag{3.6}$$

If we consider the steady-state case without a series connected reactor and note that the magnitude of the TSC current is determined by:

$$I = VB_C \tag{3.7}$$

Comparing (3.6) and (3.7) we notice that adding the reactor L amplifies the current by $n^2/(n^2 - 1)$. As n is determined by X_L and X_C, shown in (3.4), the LC circuit have to be carefully designed to avoid resonance. This is normally done by keeping the inductor reactance X_L at 6% of X_C [11].

Careful design of the TSC can thus avoid a resonance with the connected grid. However, the oscillatory component of the current (3.2) is still something that has to be taken care of. The following section provides some insight into how these currents could be limited to a minimum.

Switching operation of the TSC

To avoid the transients in the second part of (3.2), the following two conditions have to be fulfilled simultaneously [35, 36]:

$$\cos(\alpha) = 0 \tag{3.8a}$$

$$V_{C0} = \pm V\frac{n^2}{n^2 - 1} = \pm IX_C \tag{3.8b}$$

Fulfilling (3.8a) means that the thyristor switch must be closed at the positive or negative peak of the grid voltage, i.e. when $dv/dt = 0$. The second condition (3.8b) states that the capacitor has to be charged to some predetermined value when switched.

In practice it is very hard to achieve switches that are completely transient free and the objective and the actual firing strategies are instead focused on minimizing the oscillatory transients. This is done by switching the TSC when the capacitor voltage is equal to the grid voltage, if $V_{C0} < \hat{V}$, or at the peak of the grid voltage when the thyristor valve voltage is at a minimum, if $V_{C0} \geq \hat{V}$ [35]. Note that $\hat{V}$ is the peak value of the grid voltage.

Thyristor switches can only be turned off at zero current [32], which entails leaving a voltage across the capacitor equal to its peak value:

$$V_{C0} = V\frac{n^2}{n^2 - 1} \tag{3.9}$$

This leads to an increased voltage stress of the thyristor valve as the voltage across it will vary between zero and the peak-to-peak voltage of the supply.

TSC realisation and configuration

To get a smoother control of the reactive power injection, the TSC is generally split up into multiple units that can be switched into operation individually. An example of this practice is shown in figure 3.2. To achieve an even smoother control, a possible configuration would be to rate $n - 1$ capacitors for susceptance B and rate one capacitor

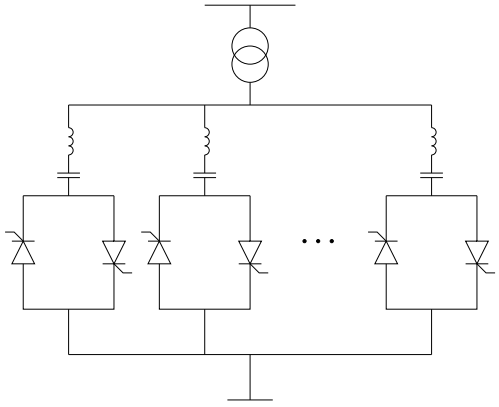

Figure 3.2: One-line diagram of a general TSC system.

for susceptance $B/2$. By using this configuration the total control steps of the TSC can be increased to $2n$ [36].

The $V - I$ characteristics of a TSC is illustrated in figure 3.3, where the discrete nature of the TSC operation is shown. This TSC configuration uses three capacitors to regulate the voltage within a range given by $V_{ref} \pm \Delta V/2$. A reasonable voltage interval has to be chosen in order to avoid switching the capacitors of the TSC too often.

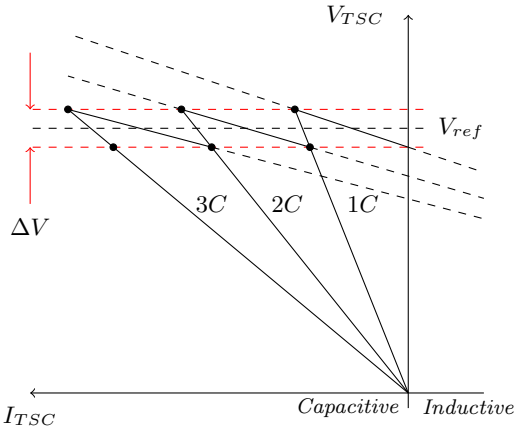

Figure 3.3: $V - I$ characteristics of a TSC configuration using three capacitor branches.

3.1.2 Thyristor switched reactor

The thyristor switched reactor (TSR) is a shunt-connected reactor in series with a thyristor valve that is used to switch the reactor ON or OFF [31]. A one line diagram of a TSR is shown in figure 3.1(a).

Basically, the TSR fulfills the same purpose as the shunt-connected mechanically switched reactor which has been employed in the AC transmission system since its early days. The only difference between these two components is that the former uses a thyristor to switch the reactor in and out of operation, while the latter uses a mechanical switch. Compared to the mechanical switch, the thyristor allows the switching process to be a lot faster [36]. Another advantage is that it will not face the same limitations on wear and tear as a mechanical switch, which is only capable of a finite number of switches. The higher investment cost could possibly be earned by the reduction in service

and maintenance costs of the mechanical switches.

As the switched reactor is not a common component in SVC installations, only this short description is provided for the sake of completeness. The controllable reactor is a much more useful and common component and this will be described in the following section.

3.1.3 Thyristor controlled reactor

The thyristor controlled reactor (TCR) can be represented by the same one-line diagram as for the previously mentioned TSR, shown in figure 3.1a. By enforcing partial conduction of the thyristor valve, the effective reactance of the inductor may be varied in a continuous manner [31].

This is achieved by controlling the firing angle α of the thyristor valve, thus controlling the TCR susceptance and its ability to absorb reactive power. As the firing angle can be varied continuously from zero to full conduction, the field of operation of the TCR is much greater compared to the discretely switched TSR.

The operation range of the firing angle lies between 90° and 180°, which respectively corresponds to full conduction and no conduction. Operating within the firing angle interval, $0° \leq \alpha < 90°$, introduces a DC offset to the reactor current which disturbs the thyristor valve [36]. Thus, this interval should be avoided.

We assume that a TCR branch with inductance L is connected to the AC voltage given by:

$$v(t) = V \sin(\omega_0 t) \tag{3.10}$$

The voltage induces a current through the reactor described by the differential equation

$$v(t) = L\frac{di}{dt} \tag{3.11}$$

which, via integration, provides the expression of the TCR current

$$i(t) = \frac{1}{L}\int_{\alpha}^{\omega_0 t} v(t)dt = \frac{1}{L}\int_{\alpha}^{\omega_0 t} V \sin(\omega_0 t)dt = -\frac{V}{\omega_0 L}\cos(\omega_0 t) + D \tag{3.12}$$

where D is a constant of integration.

The two intervals of conduction for the thyristor valve are

$$\alpha < \omega_0 t < 2\pi - \alpha \tag{3.13a}$$

$$\pi + \alpha < \omega_0 t < 3\pi - \alpha \tag{3.13b}$$

where (3.13a) is the positive half period and (3.13b) is the negative.

We calculate the TCR current (3.12) by determining the integration constant D for the two intervals in (3.13), which gives us the following:

$$i(t) = \frac{V}{\omega_0 L}\left(\cos(\alpha) - \cos(\omega_0 t)\right) \tag{3.14a}$$

$$i(t) = -\frac{V}{\omega_0 L}\left(\cos(\alpha) + \cos(\omega_0 t)\right) \tag{3.14b}$$

Figure 3.4 shows the reactor current for three different firing angles. Full conduction is achieved at $\alpha = 90°$ and the reactor current decreases as α increases. This can easily be seen as currents corresponding to $\alpha = 90°, 120°$ and 150° are plotted together with the grid voltage $v(t)$.

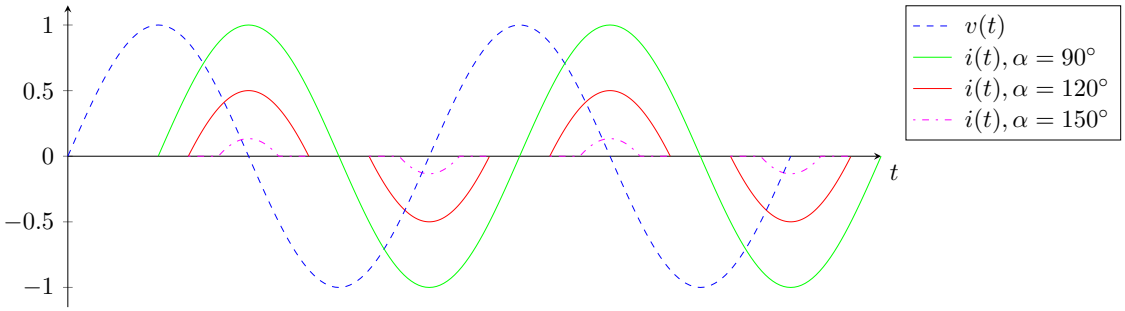

Figure 3.4: Current through the TCR for different firing angles α, with the applied voltage shown as the blue, dashed line.

TCR operation

The susceptance of the TCR, as seen by the grid, can be determined as a function of α as [35]:

$$B_{TCR}(\alpha) = \frac{1}{\omega_0 L}\left(1 - \frac{2}{\pi}\alpha - \frac{1}{\pi}\sin(2\alpha)\right) \tag{3.15}$$

Using (3.15), we can determine the amount of reactive power the TCR absorbs as:

$$Q_{TCR}(\alpha) = B_{TCR}(\alpha)V^2 \tag{3.16}$$

The operating range of the TCR is determined by its susceptance, which is a function of the thyristor angle, α. A TCR could thus be operated within the dashed area shown in figure 3.5 by varying α. It is limited by the voltage and current rating of the thyristor valve (V_{max} and I_{max}). If we compare the $V - I$ characteristics of the TCR in figure 3.5

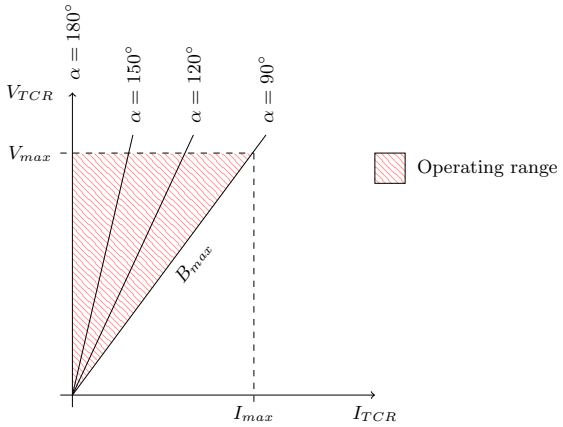

Figure 3.5: $V - I$ characteristics of the TCR.

to the characteristics of the TCR shown in figure 3.3, we can see why the TCR is a useful SVC component. Since the TSC only operates along the discrete lines defined by its total susceptance, we could use a TCR to enable continuous operation between the switched capacitors.

3.2 Common SVC topologies

Section 3.1 introduced the common building blocks used to design an SVC. The general SVC installation comprises two ranges of operation; inductive and capacitive. When designing the SVC we need to consider both the required control performance and cost of the potential components.

As the SVC is usually designed to be continuously operated, we would need a TCR in the installation. Adding a TCR will introduce harmonics to the SVC current [35]. To minimize the injection of harmonics caused by the TCR, a filter network is usually included in the SVC installation. A one-line diagram of such a filter network is shown in figure 3.1(c), alongside the other SVC building blocks in section 3.1.

In many SVC installations, a shunt connected fixed capacitance (FC) is used to inject reactive power to the grid as this would provide a cheaper solution. The fixed capacitance is usually partly or fully substituted by the filters used to dampen the TCR induced harmonics [35]. Using this FC-type configuration would not need the expensive thyristor valves and could thus be equipped with a simpler control equipment compared to the TSC described earlier in section 3.1.1.

Considering the FC-TCR type SVC, it can be noted that losses will increase as we increase the current through the TCR [35]. Therefore it is usually installed where the output is mostly capacitive as in e.g. industrial applications for power factor control [35].

Combining the TSC and TCR to make up the SVC would be a more advantageous approach for transmission system applications. This configuration makes it possible to minimize the losses by dividing the total capacitance into a number of thyristor switched capacitances. This allows us to minimize the current through the TCR and will thus minimize the losses.

To summarize, the most common topologies when designing SVC systems are:

- fixed capacitors & thyristor controlled reactor (FC-TCR)
- thyristor switched capacitors & thyristor controlled reactor (TSC-TCR)

3.3 Control application and modelling

Before we can focus on the simulation study we need to address how to properly represent the SVC in computer simulations. Models must be determined for both static and dynamic power system simulations. In this section we will present both general models and how the SVC can be represented in PSS^{TM}E.

A few assumptions have been made that should be kept in mind when considering the models presented in the succeeding sections. These assumptions are valid unless stated otherwise:

i. The devices are considered lossless.

ii. Harmonics are being neglected, only the fundamental component is considered.

iii. Balanced operation is assumed, i.e. only the positive sequence component is considered.

3.3.1 Steady-state model

This section presents how an SVC could be modeled in the steady-state load flow studies. Basic models for steady-state representation of an SVC can be based on either generators or shunt connected capacitors and reactors. Modelling the SVC based on a generator will cause problems when the SVC is operating at its reactive power limits [37].

To avoid these problems, the SVC will be modeled as a variable susceptance in this thesis.

PSS™E implementation

When we consider the load flow simulations, PSS™E provides support for modeling the SVC both as a switched shunt or as a generator. Siemens PTI recommends the switched shunt implementation [38] and this is applied here.

The SVC is implemented as switched shunts at a dummy bus connected to the high voltage bus through a zero impedance transmission line as shown in figure 3.6. This implementation was done to enable PSS™E to perform measurements of the reactive power exchange between the grid and the SVC.

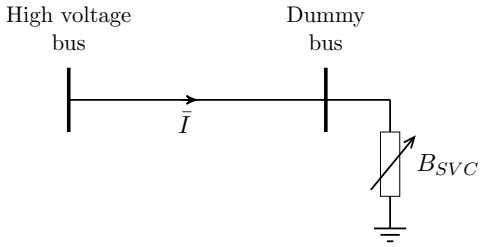

Figure 3.6: SVC implemented in the load flow case as a variable shunt susceptance.

The switched shunts are set to control the voltage at the high voltage bus and to operate in continuous control mode within a set voltage band. Their reactive power output is limited by their rating, e.g. ± 200 MVAr.

3.3.2 Dynamic modelling

SVCs are mainly used for voltage regulation at a specified bus, the controller can however also be tuned to dampen electromechanical oscillations. As we focus on voltage stability and control in this thesis, the reader is referred to e.g. [8, 35, 37], for a description on how SVCs can be used to dampen oscillations.

Dynamic modeling of an SVC could be done with a number of different approaches with varying level of complexity. However, for the kind of preliminary studies carried out within this thesis, the IEEE recommends using basic models [37]. One of the basic models recommended by the IEEE is the "Basic Model 1", presented as a very general block diagram in figure 3.7. The voltage regulator block in figure 3.7 represents the dynamic model presented in figure 3.8. This simple regulator model is also suggested by the IEEE [37].

For a more detailed modelling approach the reader is referred to e.g. [39].

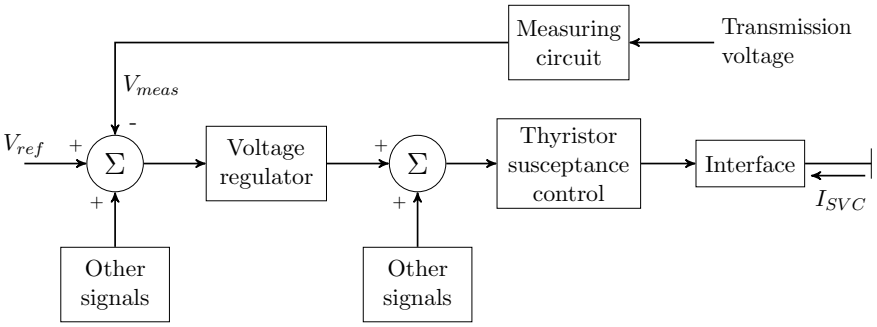

Figure 3.7: Block diagram representation of the IEEE basic model 1.

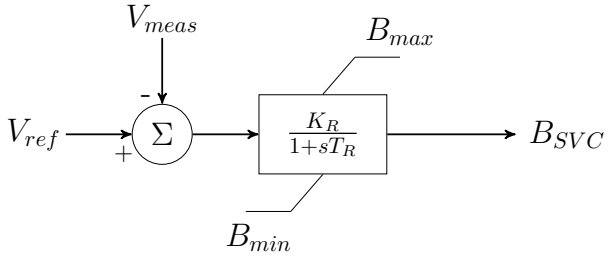

Figure 3.8: Block diagram of the voltage regulator used in the IEEE basic model 1.

Dynamic model implementation in PSS™E

Here, one dynamic model used to represent the SVC in PSS™E is introduced. The model has been developed by Siemens PTI and is delivered with PSS™E.

This dynamic SVC model, referred to as the CSSCST model, represents the SVC as a switched shunt in the load flow. It is realised as an integrator type controller and the block diagram representing the model is shown in figure 3.9.

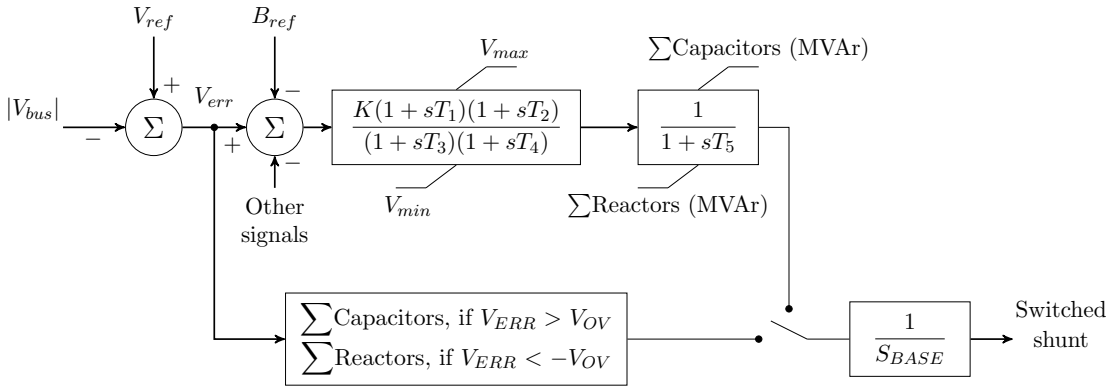

Figure 3.9: Block diagram of the SVC model CSSCST provided in PSS™E.

A lead-lag block with the time constants $T_1 - T_4$ is used to represent the voltage control. By tuning this lead-lag block, the controller can be set to achieve the required performance. The next block represents the thyristor susceptance control and the time constant T_5 represents the time delay of the SVC thyristor bridge.

If we compare the IEEE model in figure 3.7 with the PSS™E model CSSCST in figure 3.9, it can be noted that the PSS™E model design is similar to the suggested IEEE basic model. As the CSSCST model is both of the recommended basic design as

well as readily available to all PSS™E users, it has been chosen as the studied dynamic SVC model in this thesis.

3.4 Grid placement

When determining where the installation of an SVC would have the greatest effect, previous studies [20, 40] suggest that FACTS devices have the greatest impact if installed at the weakest buses of the grid.

The weak buses of the power system can generally be identified using different methods, e.g. modal analysis [21] or sensitivity analysis [22–24]. This thesis focuses on identifying weak buses using different sensitivity indices as mentioned earlier in the thesis limitations in section 1.4.

In sections 2.2.3 and 2.2.4, methods and indices were introduced that can determine which buses are prone to suffer a voltage collapse. These buses are considered the weakest buses of the power system and will be investigated further as possible SVC locations in the simulation study.

Chapter 4

Case study

This chapter presents a case study which aims to examine how power transfer may be increased by implementing additional SVCs in the grid. We are interested in increasing the transfer across the transmission interface SE2-SE3 shown in figure 4.1. Increasing the transfer limit of this particular interface will enable additional transfer of power from the northern hydro power plants to the major load centers in the south.

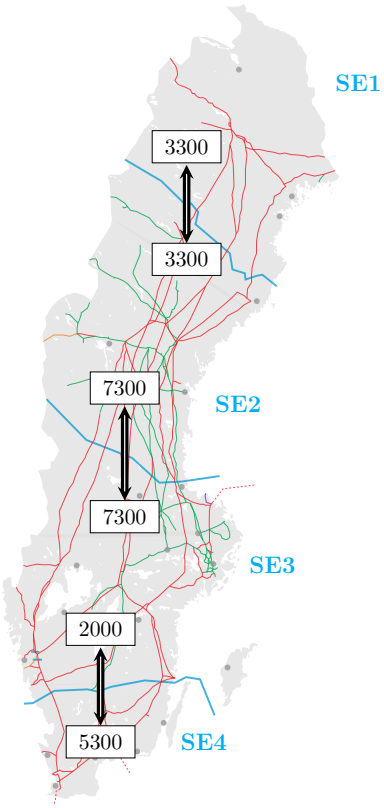

Figure 4.1: The Swedish national grid with its three transmission interfaces marked as blue lines alongside its maximum net transfer capacity (NTC) [41].

To start with, section 4.1 presents some considerations regarding the power system model and how the simulation studies will be approached. In section 4.2 we will familiarize ourselves with ways to determine a suitable location for an SVC installation. Section 4.3 presents methods for choosing a suitable set of contingencies. Finally, these contingencies are used in the dynamic simulations presented in section 4.4.

4.1 Simulation methodology

The simulations carried out in this master thesis were performed using the power system simulation tool PSS^{TM}E 31.0.1 developed by Siemens PTI. A detailed model of the Nordic power system was provided by Svenska Kraftnät. This model comprised dynamic models of generators, HVDC connections, governors, exciter systems with over-excitation limiters (OXL), load tap changing (LTC) transformers, SVCs, switched shunts and loads. Connections to neighboring countries have been modelled as equivalent constant active power loads in the static load flow representation.

The base load flow case, which all simulations have been based on, was set up as a high load case which should correspond to the grid as it existed in 2007 on a cold winter day. Note however that it was not considered to represent an extreme load case.

This case has been verified by Svenska Kraftnät to ensure stable operation for dynamic simulations and voltage collapse simulations. Note also that these simulations were successfully run for a duration of 600 s. This is important in order to ensure that the case can be used to simulate slow acting dynamics such as voltage collapse situations.

The base load flow case will be used as a reference case and will be referred to as the "base case" throughout the rest of the thesis. Power transfer data between the Swedish market areas, for this base case, is presented in appendix A.

It is important to note that the dynamic simulations performed in this thesis have been done with a certain emergency protection system enabled. This protective system is used to alter the power transfer on certain HVDC interconnections in case of a critical operating situation. Throughout this report, references to the "emergency protective system" or just "protective system" refers to this emergency protective system if not explicitly stated otherwise.

When the net transfer capacity (NTC) of the different interfaces is determined practically by TSOs, this emergency protection system has to be disabled. Activating the protective system affects the countries connected to Sweden via the HVDC lines. Svenska Kraftnät and the other TSOs have thus decided on strict regulations regarding when the system may be used. Increasing the SE2-SE3 transfer capacity, as studied in this thesis, is naturally not considered as an acceptable situation where the protective system may be activated.

The interface transfers presented in this case study deviates a lot from the existing NTC values presented in figure 4.1, due to this protection system.

4.1.1 General simulation considerations

All of the dynamic simulations are simulated for 600 s to capture the slow acting voltage dynamics. In order to save some computation time, the simulations are cancelled before 600 s if no tap change has been recorded for 180 s (this is regarded as a stable operating point) or if some "unacceptable operating situation" occurs.

An operating situation is defined to be unacceptable when one of the following conditions applies:

- the voltage level of a 400 kV bus is lower than 0.875 p.u. for at least 5 s
- the voltage level of a 220 kV bus is lower than 0.775 p.u. for at least 5 s
- the solution failed to converge within 20 iterations

These simulation parameters have been defined by Svenska Kraftnät and are applied for all the dynamic simulations performed in PSS^{TM}E.

It is desirable to perform simulations based on a number of different load flow cases. These cases are prepared with a varying SE2-SE3 interface transmission. By varying the transfer across this interface, we can determine how the system is responding to the increased stress.

To achieve an increased transfer across SE2-SE3, the generation of active power is increased in the northern market areas NO3, NO4, SE1 and SE2. To force this additional power south across the studied interface, the loads in market area SE3 are increased.

However, the available generation capacity of the northern market areas is not enough to stress the system sufficiently. In order to achieve an additional increase in power transfer, the loads in market areas SE1 and SE2 were decreased while the loads in area SE3 were increased. Note that all the loads are scaled at constant power factor ($\cos\varphi$).

4.1.2 Simulation considerations setting up a voltage collapse scenario

To accurately simulate a voltage collapse situation, some extra care is taken when the simulations are set up. Additional dynamic models are added to describe the tap changing of LTC transformers and the limiting effect of the OXLs on the reactive power production of the generators.

Note that there is a set time constant for the tap ratio control of the LTC transformers. This time constant is defined to delay the action of the tap changing in order to allow other compensation devices to act first. In effect, this will avoid unnecessary frequent switching and thus prolong the lifetime of the transformer due to decreased mechanical wear [8, 42]. For the Swedish power system, this time constant is generally set to 30 s.

LTC transformers are already installed between different voltage levels in the grid, e.g. 400/135 kV, 135/40 kV, 40/10 kV. To simulate a voltage collapse situation, additional voltage levels has to be added alongside the existing 400, 220, 135 and 77 kV levels. This is done by moving every load greater than 1 MVA to a lower voltage level (40 kV) via a 65-step LTC step-down transformer. The loss of the original load must then be adjusted to balance out the additional loss of the step-down transformer. This way the power grid will see the same load as before the step-down transformers are added.

As we noted in section 2.3.1 earlier, the operation of LTC transformers could have a major effect on voltage stability.

4.2 Identification of suitable location for SVC installation

As was mentioned in section 3.4, an SVC would have the greatest impact if installed at the weakest bus of the grid. This section presents simulations which have been performed to identify the weakest buses in the SE2-SE3 interface vicinity.

This simulation study has focused solely on the 400 kV buses in the Swedish national grid and all of the studied buses are already existing buses.

Market area SE2 contains around 15 buses at the 400 kV level and 9 of these were included in this study. The SE2 buses excluded are located in the northern part of SE2 closer to the SE1-SE2 interface. They were therefore considered to have a smaller influence on the studied SE2-SE3 interface compared to the chosen buses.

In market area SE3, the 24 chosen buses forms a clear majority of the existing 400 kV buses in the area. The excluded buses are mainly located in the southern part of

SE3, bordering SE4 and therefore considered to have a smaller influence on the studied interface.

A set of 33 buses were selected as possible candidates and the $VCPI$ index and Q-V sensitivity were calculated for each of them.

- Buses 1–9 are located in market area SE2
- Buses 10–33 are located in market area SE3

This set of possible candidate buses were chosen to narrow the scope of the thesis somewhat and limit the amount of performed simulations and calculations. However, this chosen subset of the Swedish 400 kV buses still includes almost every single 400 kV bus in the vicinity of the SE2-SE3 interface.

4.2.1 Identification based on Q-V sensitivity

The Q-V sensitivities were calculated based on the Q-V curves presented in section 2.2.2 as well as the descriptions of sensitivity analysis in section 2.2.3.

The Q-V curves were simulated using the "QV Analysis" tool in PSS™E. To avoid computational problems the simulations have been performed with the LTC transformers in a locked tap position. The switched shunt reactors and capacitors were all enabled in the simulations and the apparent power output limiters (VAR limiter) of the generators were set to apply immediately.

Some of the studied buses already had some equipment installed to control the bus voltage, e.g. a switched shunt or an SVC. In these cases, the controllable equipment has to be switched to a locked state in the power flow case. Otherwise their operation will interfere with the solution. This is problematic as the voltage varies into the range in which the controllable component is operable. This interference causes computational problems in PSS™E which in some cases aborts the simulations.

The Q-V sensitivity was calculated as a linear approximation of the positive slope of the Q-V curve:

$$\frac{\Delta Q}{\Delta V} = \frac{Q_{max} - Q_{min}}{\Delta V} \tag{4.1}$$

As can be seen in figure 4.2, the linear approximation of the positive slope is close to the slope of the simulated curve.

The buses with the ten steepest slopes, i.e. the ten "weakest" buses, are presented in table 4.1. See appendix B for the complete list of calculated Q-V sensitivities for all of the 33 studied buses.

The buses in table 4.1 are either located near a major load area in SE3 or in the vicinity of the SE2-SE3 interface. However, most of them are close to the major load area in market area SE3. This indicates that this particular part of the grid may benefit from additional reactive power compensation.

4.2.2 Identification based on $VCPI$

The voltage collapse proximity indicator ($VCPI$), described in section 2.2.4, was calculated using a load flow case with a highly stressed SE2-SE3 interface. This case, from now on referred to as the "$VCPI$ case", had an SE2-SE3 interface transfer of 8600 MW. For more information regarding the transfer data between the simulated market areas, see appendix A.

The $VCPI$ case represents how the reactive power generation will be distributed amongst the generators when the system is heavily stressed. This is of importance as we

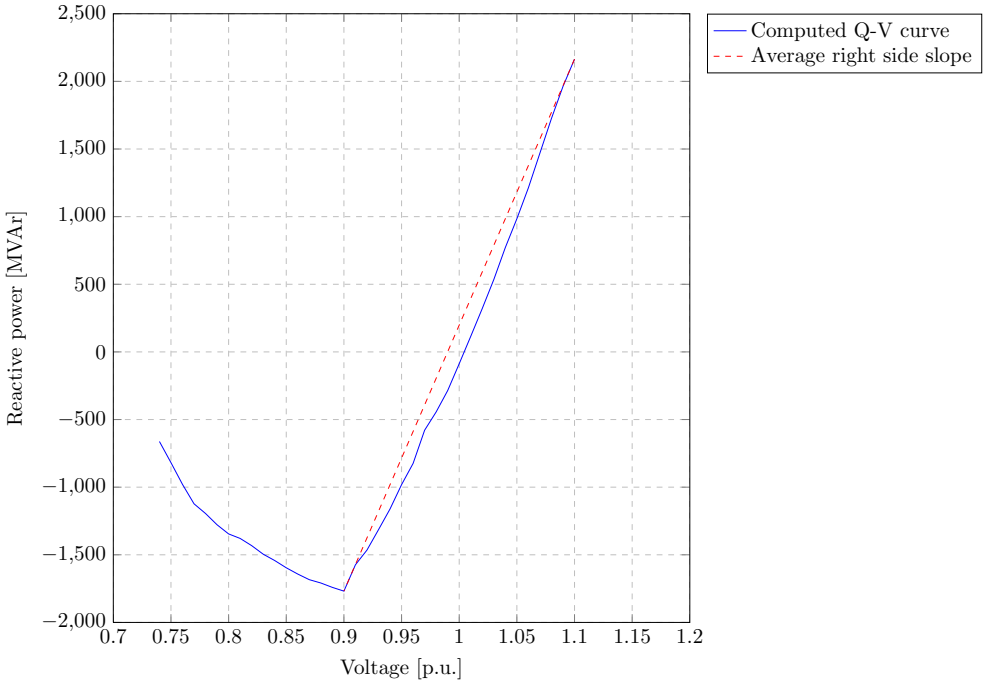

Figure 4.2: Example of a simulated Q-V curve, presented alongside its average slope.

Table 4.1: The ten buses with the largest Q-V sensitivities.

Rank	Bus number	Slope [MVAr/p.u. voltage]
1.	23	19 664
2.	19	18 864
3.	6	18 549
4.	20	15 576
5.	2	15 182
6.	17	14 884
7.	8	14 230
8.	16	13 565
9.	21	13 344
10.	30	12 488

are interested in locating the bus where reactive power injection would have the greatest effect when the system approaches a collapse situation.

Calculating the $VCPI$ for a case with a low interface stress would give a completely different result. Thus indicating a different, less suitable candidate bus for reactive power injection with regards to voltage collapse prevention.

To calculate the $VCPI$, a fictitious purely inductive 1 MVAr load is connected to the studied bus i ($\Delta Q_i = 1$ MVAr). Load flow calculations are performed before and after the connection of the 1 MVAr load. The total increase in reactive power generation, ΔQ_j, is measured at every generator bus j, connected to the Nordic power system. This is done by summing the reactive power output from every active generator and calculating the increase when the additional load is connected.

See the bar graph in figure 4.3 for the $VCPI_Q$ indices of the 33 studied buses. The buses with the ten highest $VCPI_Q$ indices are ranked in table 4.2. Refer to

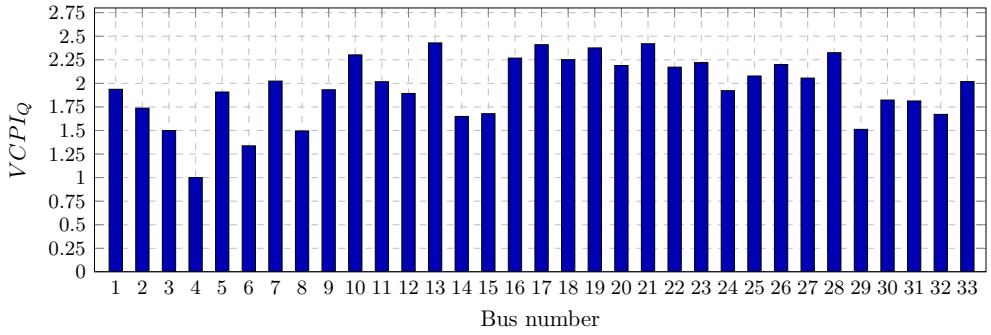

Figure 4.3: $VCPI_Q$ of the investigated buses in the high transfer case.

appendix A for the extended transfer data of the $VCPI$ case and to appendix B for the complete list of calculated $VCPI_Q$ indices of the studied buses.

Table 4.2: List of the 10 buses with the highest $VCPI_Q$ values.

Rank	Bus no.	$VCPI_{Q_i}$
1.	13	2.429
2.	21	2.420
3.	17	2.410
4.	19	2.376
5.	28	2.325
6.	10	2.302
7.	16	2.268
8.	18	2.251
9.	23	2.251
10.	26	2.200

The $VCPI_Q$ results indicates that the most suitable candidate for an SVC implementation would be bus 13, which is located at a major load area. However, the buses 21, 17 and 19 have $VCPI_Q$ values quite close to the prime candidate. Additionally, these are located geographically close to bus 13, thus it is reasonable to also investigate these buses as possible candidates.

4.3 Contingency identification

To ensure the security of a power system, it should be able to handle a large set of contingencies. Examples of such contingencies are [8]:

- permanent three-phase faults on any generator, transmission circuit, transformer or bus section, with normal fault clearing.
- loss of any element without fault.
- permanent phase-to-ground fault on a circuit breaker, cleared in normal time.

A real, large-scale power system comprises hundreds or even thousands of generators, transmission lines and transformers. This will lead us to an extensive set of possible contingencies which needs further investigation to ensure secure operation.

Before the dynamic simulations can be performed, we have to compile a set of contingencies to use in this study. This set should consist of the contingencies which are most likely to cause a voltage collapse. As we are studying the SE2-SE3 interface, the contingencies which would stress this interface the most are of particular interest. Only the most severe contingencies will be used in the following dynamic simulations.

In order to ensure that a wide range of contingencies are considered, we evaluate a large number of transmission line faults, tripped generators, transformers and busbar faults. Note that we only consider contingencies within the Swedish transmission system.

To determine the most severe contingencies, they are evaluated by how they affect the power transfer across the 400 and 220 kV lines connecting SE2 and SE3. The "AC contingency solution (ACCC)" tool in PSS™E was used for this evaluation.

Table 4.3 presents the contingencies which have the greatest effect on power transfer across the SE2-SE3 interface. These contingencies are later used as disturbances in the dynamic simulations and to determine the transmission capacity of the interface.

Table 4.3: A list of the 15 contingencies that increase the SE2-SE3 transfer the most.

ID	Contingecy type	Description
1.	Generator	Generator at a nuclear power plant
2.	Busbar	Busbar close to nuclear power plant
3.	Generator	Generator at a nuclear power plant
4.	Generator	Generator at a nuclear power plant
5.	Generator	Generator at a nuclear power plant
6.	Generator	Generator at a nuclear power plant
7.	Generator	Generator at a nuclear power plant
8.	Generator	Generator at a nuclear power plant
9.	Generator	Generator at a nuclear power plant
10.	Generator	Generator at a nuclear power plant
11.	Generator	Generator at a nuclear power plant
12.	Transformer	400 kV - 300 kV transformer, SE2
13.	Line	Transmission line, SE3
14.	Line	Transmission line, SE3
15.	Transformer	400 kV - 135 kV transformer, SE3

4.4 Results from dynamic simulations

This section presents the results from the dynamic simulations carried out throughout the work of this thesis. Section 4.4.1 determines the transmission capacity of the unaltered SE2-SE3 interface. Based on those results, we investigate how much we can increase the interface capacity by installing additional reactive compensation. This is investigated in sections 4.4.3 and 4.4.4.

4.4.1 Transfer limits of transmission interface SE2-SE3

To investigate the dynamic transfer limit across interface SE2-SE3, a set of static load flow cases are prepared where the interface transmission is gradually increased. This is achieved by scaling generation and loads as described in section 4.1.1. These load flow cases are later used in the dynamic simulation study.

To determine the stability limit of these cases, dynamic simulations are performed in PSS^{TM}E where the contingencies listed in table 4.3 are applied. This will decide the level of transfer across interface SE2-SE3 at which the grid could be prone to suffer a voltage collapse.

Simulation results from five selected static load flow cases will be presented in this section. The purpose of this is to describe how the system reacts when subjected to an increased stress that eventually leads to a voltage collapse. Table 4.4 presents the interface transfer of the five cases. For more detailed transfer data of the Swedish market areas for the different cases, refer to appendix A. Note that the case denoted "Base case" in table 4.4 is the unaltered load flow case supplied from Svenska Kraftnät described in section 4.1.

Table 4.4: The five simulated cases and their level of transfer across SE2-SE3.

Case description	SE2-SE3 transfer [MW]
Base case	5750
Case 1	8500
Case 2	8600
Case 3	8650
Case 4	8700

In figure 4.4 we can see how the voltage profile at bus 2 is affected by the increasing interface transfer following a simulated contingency. Bus 2 is located close to the SE2-SE3 interface and it is fairly close, electrically, to the buses indicated as weak by the Q-V and $VCPI$ indices.

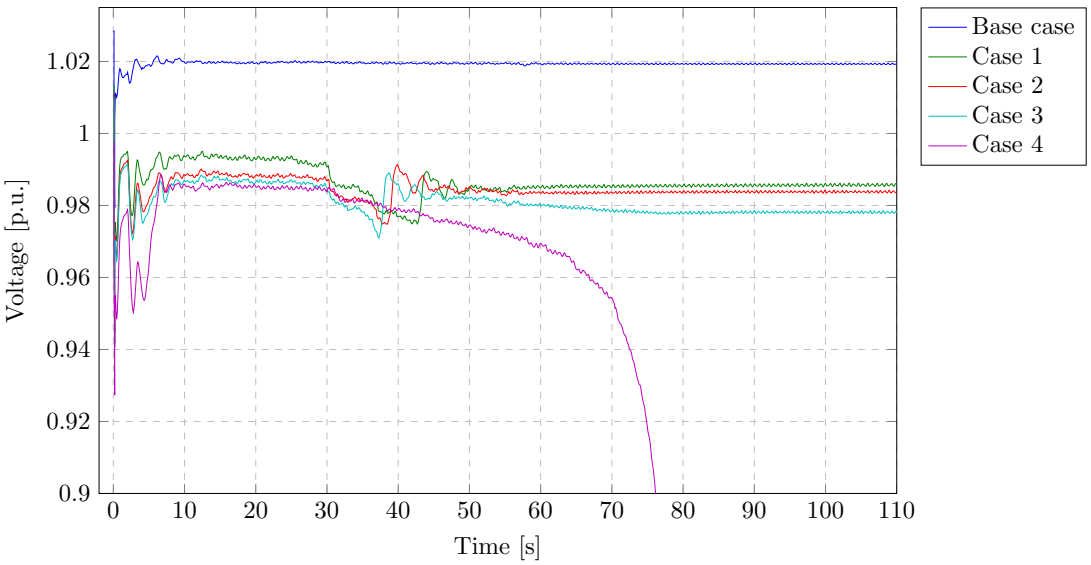

Figure 4.4: Voltage profiles of bus 2 following a nuclear generator fault at $t = 0$ s and disconnection of the generator after 100 ms.

The presented data results from a simulated fault applied at a nuclear generator. After 100 ms the fault was cleared and the generator was simultaneously disconnected from the grid. This fault is labelled as contingency 6 in table 4.3 shown earlier.

As we can see in figure 4.4, the base case is the least affected by the simulated contingency, which is to be expected. The voltage level stabilizes at 1.02 p.u. after about 10 s. Cases 1–3 also reach a stable state of operation, but this takes about 60 s. In these cases the voltage level settles at a lower value, but still within the acceptable limits.

For cases 1–3 we can see a distinct jump in voltage level around 40 s. This is due to the activation of the emergency protective system mentioned earlier in section 4.1. We can clearly see that this protective system eases the stress of the power system as the voltage decline is aborted followed by the convergence to a stable state.

Case 4 fails to reach a stable state of operation after the faulted nuclear generator was disconnected and the system suffers a voltage collapse at around 75 s. Based on the results from this simulation study we can determine the highest, stable power transfer across the SE2-SE3 interface to 8650 MW (Case 3).

4.4.2 A closer look at the voltage collapse

As we could see in figure 4.4, the system suffered a voltage collapse for the transfer level in case 4 when subjected to contingency 6. To further increase our understanding of the voltage collapse we investigate the origin and the cause of the collapse.

Locate the origin of the voltage collapse

In an attempt to locate the origin of the voltage collapse, we study the voltage profiles at buses from all parts of the Swedish power system.

Figure 4.5 presents plots of the voltage level at 9 buses located somewhere from the northern parts of SE1 down to the southern parts of SE4. The plots in this figure refer to buses which are simply identified by the market areas in which they are located.

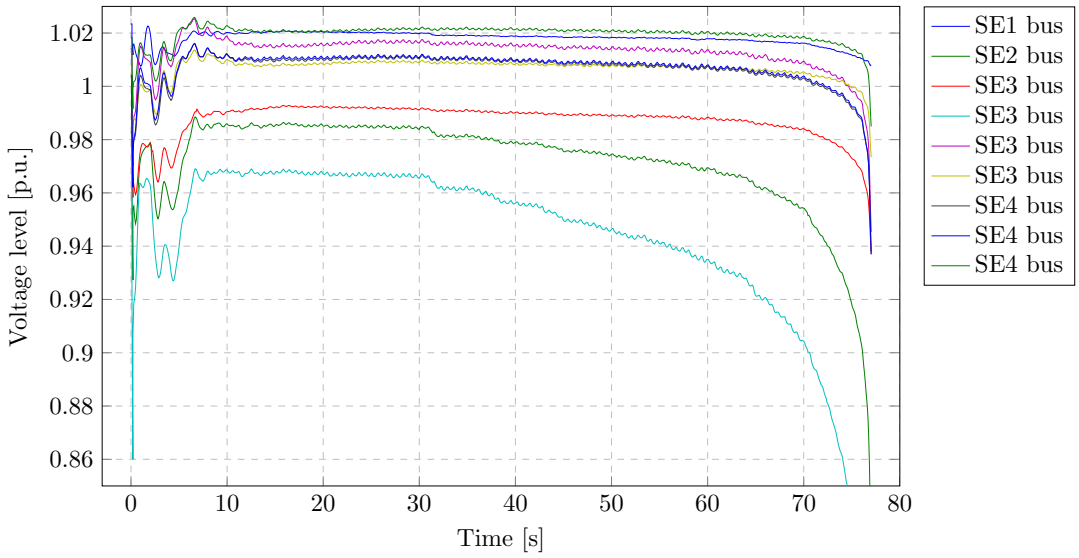

Figure 4.5: Voltage profiles at 9 buses representing different parts of the Swedish transmission system during a voltage collapse situation.

In these plots we note that the voltage level of the turquoise colored SE3 bus has the lowest magnitude and that it also decreases the fastest compared to the other bus

voltages. This gives us some indication that the voltage collapse probably has its origin somewhere close to this bus. Based on these observations, it is of interest to further investigate the 400 kV buses in its vicinity. Figure 4.6 presents the 6 voltage profiles of the 400 kV buses in this area. These 6 buses include the bus with the lowest magnitude in figure 4.5 and all are located in the same market area, i.e. SE3.

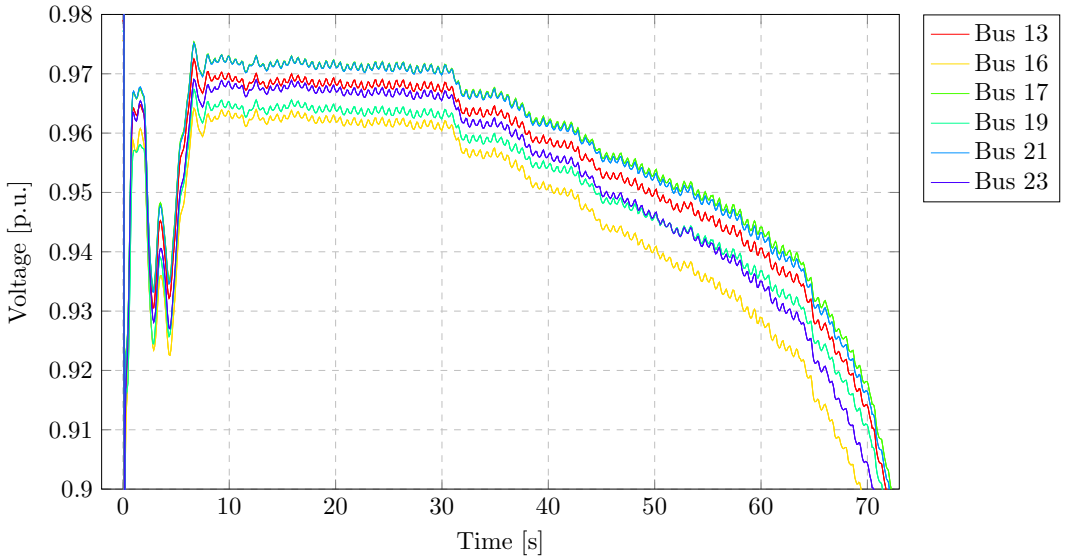

Figure 4.6: Voltage profiles of 6 buses located in SE3 during a voltage collapse.

It is interesting to compare the buses present in figure 4.6 with the results in sections 4.2.2 and 4.2.1. We notice that all 6 buses shown in figure 4.6 were listed within the ten highest $VCPI$ values listed in table 4.2. Additionally, 5 of these buses are also ranked as weak by the Q-V sensitivity index in table 4.1. This tells us that we should base our placement strategy on the weak buses listed in sections 4.2.2 and 4.2.1.

Cause of collapse

Now that we have a better insight into the origin of the voltage collapse, we can take a look at what is causing it. As we discussed earlier in chapter 2, voltage collapses stems from the inability of the system to deliver sufficient amounts of reactive power to the loads. Transfer of reactive power is limited by the inductive nature of the power system, as we could see in section 2.1.2.

If the power system is heavily stressed and, due to some contingency, the voltage level begins to drop in the distribution grid, LTC transformers begin load restoration. In section 2.3.1, we discussed how the tap changing action of these transformers would increase the strain on the transmission system. Thus, it is interesting to investigate the operation of LTC transformers and how they affect the reactive power demand of the system leading up to the voltage collapse.

Figure 4.7(a) shows the voltage profile of bus 16 for the three cases with the highest interface transfer listed in table 4.4. In figures 4.7(b)-4.7(d) we can see how the tap ratio is changed at some representative transformers in the distribution grid. Figure 4.7(e) shows how the total number of active current limiters is affected in the different transfer cases.

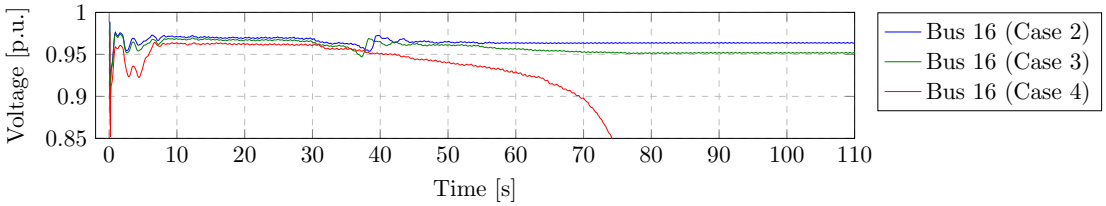

(a) Voltage profiles of bus 16 for three different transfer cases.

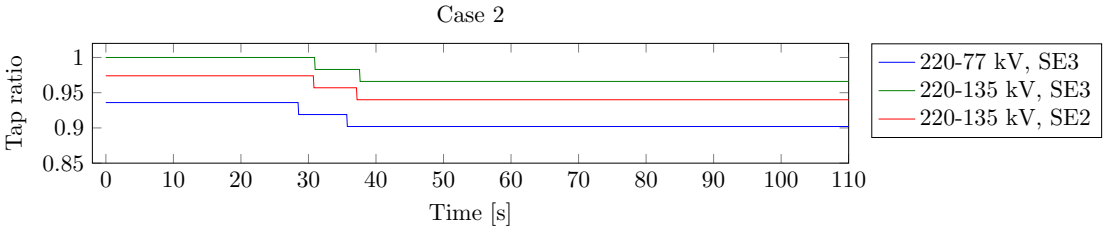

(b) LTC operation of three SE3 transformers for transfer case 2.

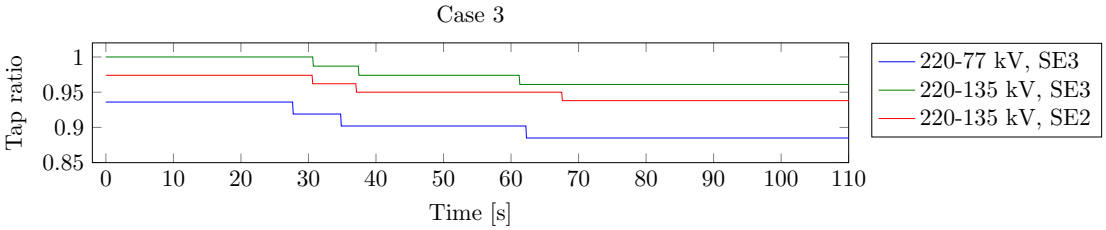

(c) LTC operation of three SE3 transformers for transfer case 3.

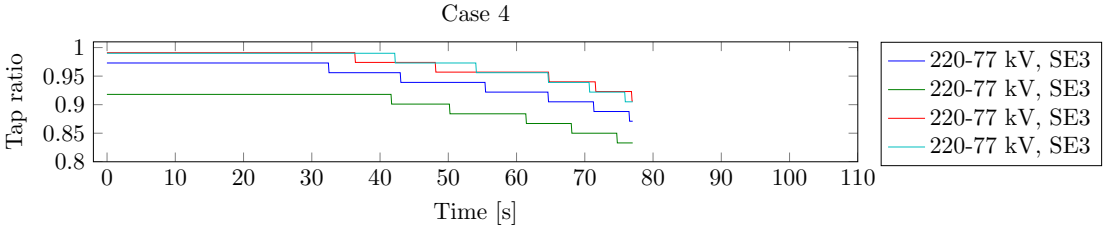

(d) LTC operation of three SE3 transformers for transfer case 4.

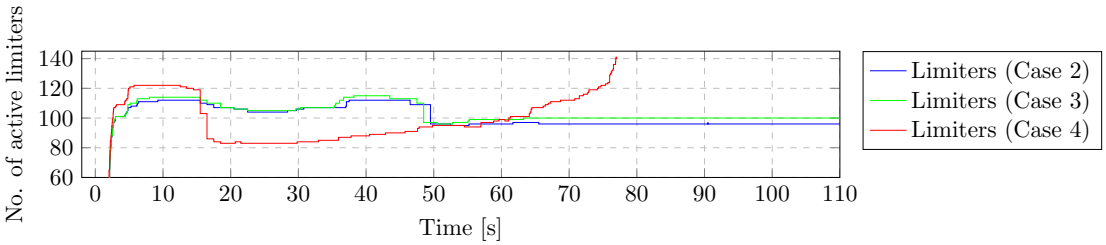

(e) Number of active generator current limiters for three different transfer cases.

Figure 4.7: Voltage profiles, LTC operation and number of active generator current limiters for three different transfer cases.

Figure 4.7(b) shows the LTC operation for case 2. Here, we can see how three transformers in the sub-transmission and distribution grid are acting to restore the voltage level. The influence of the time constant of the LTC control, mentioned in section 4.1.2, can be observed as no tap change is performed before about 30 s have elapsed. We also note that the protective system, mentioned in section 4.1, takes action after 40 s (see figure 4.7(a)) which is enough to restore the system voltage to an acceptable level. No further change in tap ratio is thus needed and the system is considered stable.

In figure 4.7(c) we see a similar process for case 3 as we did for case 2. However in this case, the protective system action does not restore the voltage level fully and another set of LTC switches are required between 60–70 s. This last action was enough to return the system to an acceptable point of operation and the system is considered stable.

Figure 4.7(d) shows the LTC action for the most stressed transfer case, i.e. case 4. Here we can see how the LTCs begin their attempt to restore the voltage level at around 30 s. However, compared to the previous cases, no protective action is able to relieve the stress of the power system. Instead, the LTCs try to restore the voltage level of the distribution grid. This increases the stress level of the transmission system and the voltage level keeps on reducing up to the point of voltage collapse. In this case, the system fails to enter a stable state and is thus considered unstable.

In figure 4.7(e), we can see how the generator current limiters are affected for the three different transfer cases. Following the applied contingency the system stress is duly increased. We can see this by noting that around 100 current limiters are activated the first couple of seconds. These generators are at this point operating at their maximum capacity and they cannot further increase their reactive support.

The system is now in a state of strained operation and after a certain amount of time we can see that the current limiters are gradually deactivated. This could indicate that the system is returning to a less stressed state of operation. However, as the voltages begin to drop in the distribution grid, the LTC operation increases the strain of the system. We can see their effect by noting that the number of active current limits are starting to increase after around 30 s.

In case 2 and 3 the activation of the protective system causes some additional generators to reach their limit between 40–50 s. This follows as the power flows in the system are affected by altering the power exchange on some HVDC interconnections. After 50 s, as the system enters a stable state of operation, the number of active current limiters is reduced.

Now focusing on case 4, we can see how the continuous switching operation of the LTCs keep increasing the number of active current limiters. As the LTC operation increases the stress on the transmission system, the reactive power demand caused by the heavily loaded transmission lines is increased, as was shown in section 2.3.1.

This further adds to the demand and more and more generators are reaching their current limits. Eventually the system cannot cope with the lack of reactive power and the voltage collapses.

4.4.3 Transfer capability with added SVCs

This section aims to determine where an SVC would have the greatest impact if placed using the different indices described in sections 4.2.1 and 4.2.2. These results were further supported by the results in section 4.4.2, which suggested that the origin of the voltage collapse is located close to the indicated buses. Finally, it is time to examine how the addition of SVCs affects the transmission capacity of the SE2-SE3 interface.

To investigate how an SVC affects the interface transfer capability, the PSS^{TM}E model CSSCST described earlier in section 3.3.2 will be used to model the SVC. The control parameters of the model are based on previous work and examples provided by Siemens PTI [17, 38, 43].

In PSS^{TM}E, the steady state gain K is entered as MVAr/p.u., i.e. to achieve a gain of 150 on a ±200 MVAr SVC, K must be set equal to:

$$K = (\text{required gain}) \cdot (\text{SVC rating}) = 150 \cdot 400 = 60000 \tag{4.2}$$

We will investigate two different SVC cases, one with a power rating equal to ±200 MVAr and one rated to ±400 MVAr. The purpose of this is to investigate how the amount of injected reactive power is affecting the interface transfer capability.

Table 4.5 shows the chosen parameter values for our two separate SVC configurations.

Table 4.5: CSSCST model parameters for two SVC configurations.

SVC rating	K [MVAr/p.u.]	T_1 [s]	T_2 [s]	T_3 [s]	T_4 [s]	T_5[s]	V_{OV} [p.u.]
±200 MVAr	60000	0	0	2.4	0	0.03	0.5
±400 MVAr	120000	0	0	4.8	0	0.03	0.5

Let us recap the results from the study of weak system buses in section 4.2 and based on this, select a set of buses to use in the simulations. Table 4.6 lists the candidate buses and their respective $VCPI$ and Q-V sensitivity rankings.

Table 4.6: Suggested SVC buses with their respective $VCPI$ and Q-V sensitivity rank.

Bus no.	$VCPI$ rank	Q-V rank
2	25	5
6	32	3
13	1	17
17	3	6
21	2	9
23	9	1
29	29	15

As can be seen, the selected buses are a set of buses ranked both high and low by both the $VCPI$ and Q-V indices. These buses have been selected to investigate how effective these indices are when deciding where to place an SVC. The indices are evaluated based on how the SVC placement affects the power transfer across the SE2-SE3 interface.

Note that the simulation methodology is the same as in section 4.4.1 where the transfer capability of the uncompensated SE2-SE3 interface was determined. Scaling of the loads and generators is done the same way and the same list of contingencies, presented in table 4.3, is applied. Though, for these simulations, an additional contingency is added to guarantee that the "$N-1$ criteria"[†] holds. Performing simulations for this contingency is necessary as the addition of the SVC have altered the grid. This new contingency is presented in table 4.7

To determine the new transfer capacity of the SE2-SE3 interface, a set of simulations

[†]The $N-1$ criteria states that the system must be able to withstand the loss of any major component without entering an unstable state of operation.

Table 4.7: Contingency added to guarantee the $N-1$ criteria when an SVC has been added.

ID	Contingency type	Description
16.	SVC fault	SVC short-circuit fault and disconnection

with increasing interface transmission have been performed. These simulations were run for each of the suggested SVC locations and the results from the simulation study are presented in table 4.8.

The results in table 4.8 shows that we would achieve the highest capacity increase by installing the SVC to either bus 13, 17 or 21. Comparing the capacity for bus 2, the increase is 50 MW less for both SVC configurations. For bus 23, on the other hand, the added capacity is 50 MW less only for the ±200 MVAr SVC configuration. Bus 6 gives an even lower increase in capacity, only 50 MW for both of the suggested SVC configurations. Finally, bus 29 performs the worst as adding an SVC to this bus would not increase the interface capacity at all.

Comparing the results in table 4.8 with how the buses were ranked by the $VCPI$ and Q-V indices. Notice that the three buses which yielded the highest increase in interface capacity; buses 13, 17 and 21, were ranked as the three weakest buses by the $VCPI$ index.

The Q-V sensitivity index on the other hand, ranked buses 23, 6 and 2 as the three weakest buses. Comparing this ranking to the simulations results in table 4.8 shows that, in our case, the SVC should be placed based on the $VCPI$ index.

Table 4.8: Results from the simulations for the different SVC placements.

Bus no.	SVC rating [MVAr]	Interface transfer [MW]	Added capacity [MW]
2	±200	8750	100
2	±400	8800	150
6	±200	8700	50
6	±400	8700	50
13	±200	8800	150
13	±400	8900	200
17	±200	8800	150
17	±400	8900	200
21	±200	8800	150
21	±400	8900	200
23	±200	8750	100
23	±400	8900	200
29	±200	8650	0
29	±400	8650	0

Figure 4.8 illustrates the operation of the added SVC for 4 of the buses with the highest increase in interface capacity. The simulated case is the previously unstable transfer case (case 4), presented in section 4.4.1. As we can see, the voltage level now stabilizes thanks to the reactive power injected by the SVC.

Adding another SVC to a weak area of the Swedish national grid have thus successfully increased the SE2-SE3 transfer capacity.

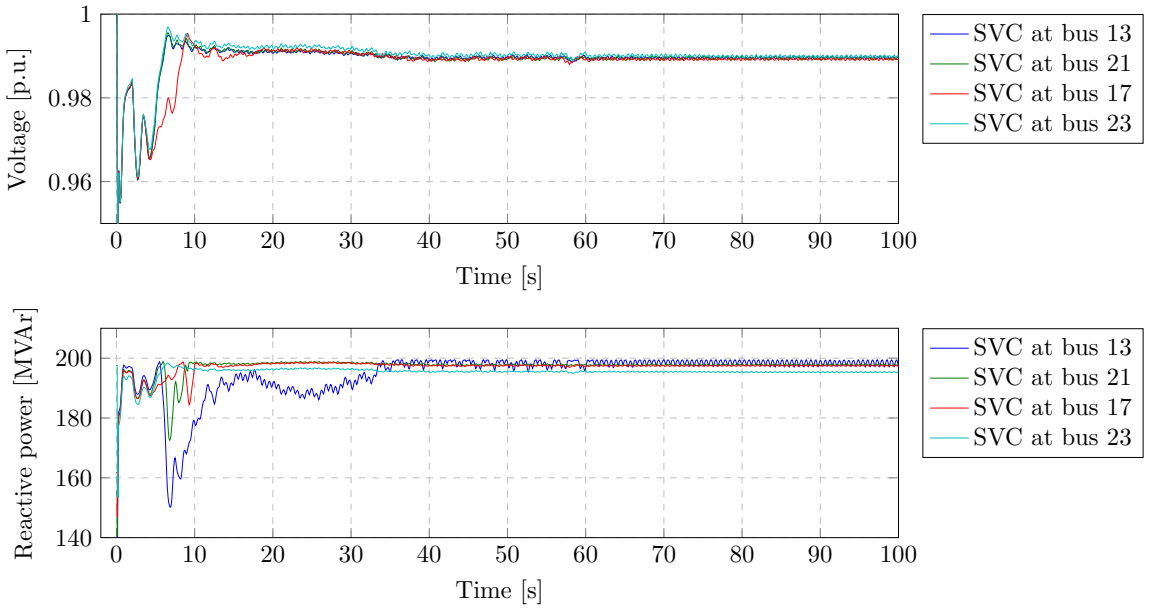

Figure 4.8: Voltage profiles at bus 2 and reactive power output of the ±200 MVAr SVC, presented for 4 different SVC locations where contingency 6 is simulated with an SE2-SE3 transfer of 8700 MW.

4.4.4 Transfer capability with switched shunt compensation

As we could see in section 4.4.3, adding an additional SVC increases the SE2-SE3 interface capacity with up to 200 MW depending on its location. To investigate the effect of the continuous control of the SVC, this section compares the performance of the SVC with regular switched shunt compensation.

This comparison study is performed on 4 of the buses that resulted the highest increase in interface capacity; buses 13, 17, 21 and 23. The ±200 MVAr SVC simulated in section 4.4.3 is replaced with switched shunts with the same power rating. The simulation methodology is the same as in section 4.4.3 and the same set of contingencies have been used to verify the results. Table 4.9 lists the results from the performed simulations.

Table 4.9: Results from the simulations using switched shunts.

Bus no.	Shunt rating [MVAr]	Interface transfer [MW]	Added capacity [MW]
13	±200	8700	50
17	±200	8750	100
21	±200	8750	100
23	±200	8750	100

The results shown in table 4.9 should be compared to the results from the case where we used an SVC, listed in table 4.8. Depending on the location of the reactive power compensation, the interface capacity is up to 100 MW higher for the SVC compared to a regular shunt installed at the same bus. It appears that the continuous control capability of the SVC enables a higher interface transfer capability.

4.5 Wind power integration and voltage stability

The addition of large wind farms to power grids introduces a set of new challenges regarding voltage stability. Basing the wind power generator on asynchronous machines increases the demand for reactive power as the induction generator consumes reactive power [44]. This additional reactive power demand is usually locally compensated by connecting shunt capacitances at the wind farm connection bus. However, as the reactive power injection by the capacitors is heavily voltage dependent, the injected power will decrease when needed the most as the voltage decreases.

To address these voltage stability challenges, the addition of an SVC close to the wind farm have proven successful [45, 46]. Adding the SVC close to a wind farm can lower the risk of a voltage collapse by supporting the increased demand for reactive power from the induction generator following a fault in the grid [44].

In order to investigate how an SVC would interact with a large (1000 MW) wind farm, a new set of load flow cases have been prepared. The wind farm has been modeled based on both a squirrel cage induction generator and a doubly fed induction generator.

4.5.1 Wind farm modeled as squirrel cage induction generators

To model the wind farm with squirrel cage induction generators, the PSS^{TM}E standard model CIMTR3 is used [38, 47]. See appendix C for the complete list of used parameters values.

The purpose is to examine how the power system reacts when a 1000 MW wind farm is connected to the system via a weak connection bus. Bus 13 was chosen as the connection bus for the wind farm as it was previous identified as the weakest bus, based on the $VCPI$ index in section 4.2.2. The wind farm comprises 11 large induction generators connected to a dummy bus, which is again connected to the high voltage transmission system via a lossless transmission line. A shunt connected 280 MVAr capacitor is added to the wind farm connection bus to compensate for the steady state reactive power demand of the wind turbine generators. The load flow data of the induction generators is listed in appendix C.

As the power system has been greatly modified by adding the large wind farm, the interface transfer limit of SE2-SE3 has to be redetermined. This was done using the same simulation methodology as previously presented in section 4.4.3. Table 4.10 lists the SE2-SE3 interface transfer for three of these prepared load flow cases.

Table 4.10: The simulated cases and their level of transfer across SE2-SE3.

Case description	SE2-SE3 transfer [MW]
Case 1	6700
Case 2	6850
Case 3	6900

To determine the highest stable interface transfer, the contingencies listed in table 4.3 were each applied. Another contingency related to a fault at the wind connection bus was added to ensure the $N-1$ criteria. This contingency is presented in table 4.11.

Table 4.11: Contingency for the $N-1$ criteria when a wind farm has been connected.

ID	Contingency type	Description
17.	Wind farm fault	Fault at connection bus and disconnection of wind farm.

Figure 4.9 shows the voltage profiles at bus 2 when contingency 14 has been applied to each of the transfer cases. As can be seen, the highest possible interface transfer is determined for case 2 and is equal to 6850 MW. Note that the increase in voltage for case 3 at about 145 s, is again caused by the activation of the emergency protective system mentioned earlier in section 4.1.

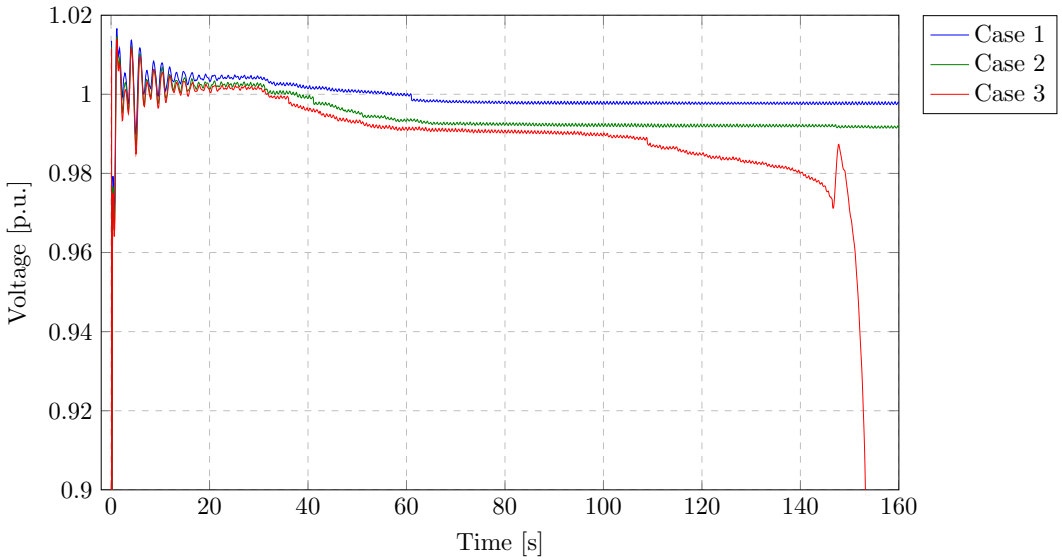

Figure 4.9: Voltage profiles at bus 2 when contingency 14 was applied at $t = 0$ s and cleared after 100 ms.

Based on these results we can conclude that adding a 1000 MW induction generator based wind farm to SE3 will have a significant impact on the SE2-SE3 transmission capacity. Recalling the original SE2-SE3 capacity of the unaltered power system in section 4.4.1, we note that adding the new wind farm has lowered the capacity by 1800 MW. Adding this new wind farm will thus alter the dynamics of the studied power system.

It is therefore interesting to investigate the cause of the voltage collapse in case 3. The simulated contingency which drives the system to a voltage collapse situation is contingency 14, a faulted transmission line tripped after 100 ms. At the time of the fault this line is heavily loaded and when the line is tripped, a large amount of power must be redistributed to the adjacent lines. This additional power transfer increases the losses and the reactive power consumption of the transmission lines as mentioned earlier in sections 2.1.1 and 2.3.1.

Adding a wind farm based on squirrel cage induction generators will contribute to the increased reactive power demand following certain contingencies. If, e.g. a short-circuit fault occurs close to the wind farm connection, the voltage level at the connection bus will drop rapidly, causing the electrical torque of generators to decrease. If the mechanical torque caused by the force of the wind stays constant, the generator will accelerate causing the generator slip to increase. Operating the generators at this increased slip,

plus the inductive current drawn from the grid in order to build up the magnetic field of the generators will increase the reactive power consumption of the wind farm after the fault has been cleared [48].

To visualize how the reactive power demand is affected, the voltage profile and reactive power exchange for the wind farm is presented in figure 4.10. Note that contingency 14 has been applied in these simulations as well. Here we can clearly see the large demand

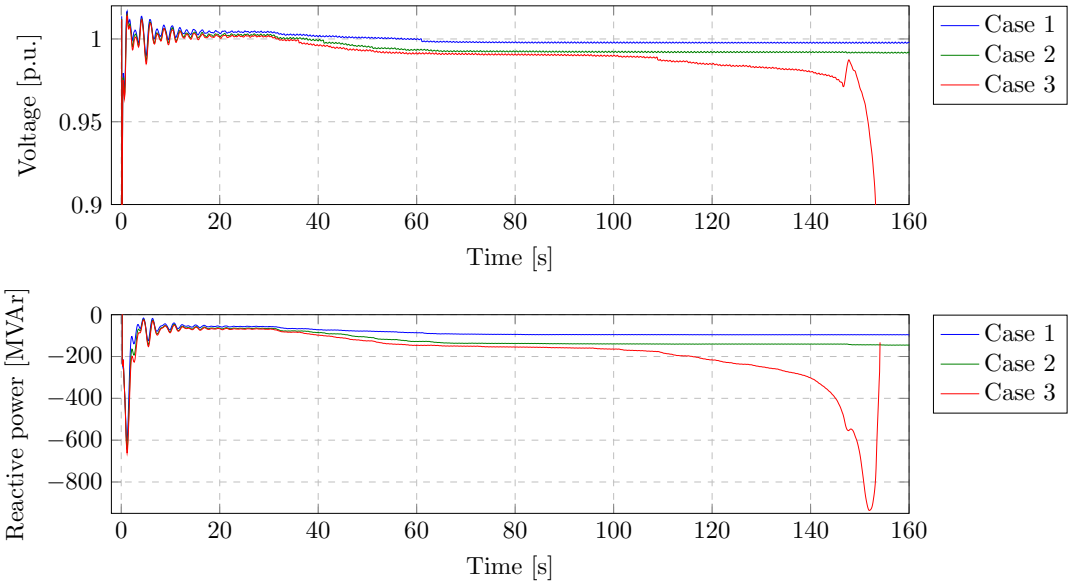

Figure 4.10: Voltage profile and reactive power exchange for the wind farm modeled as induction generators.

for reactive power after the fault has been cleared at $t = 0.2$ s. In figure 4.10 the reactive power exchange curve for case 3 shows a demand of more than 600 MVAr for a short period.

The voltage level then starts to decrease after about 30 s and at the same time the reactive power consumption of the wind farm increases slightly. If we take a closer look into the LTC transformer action and current limiters as we did earlier in section 4.4.2. Figure 4.11 shows the operation of the LTCs and how the number of active limiters are affected when contingency 14 is applied.

The LTC transformers begin to operate at around 30 s to attempt to restore the loads. They finish their operation at about 60 s for all the three cases and enters a stable operating state for case 1 and 2. In case 3 the system also seems to have entered a stable state, until the LTCs begin to operate around 110 s.

In case 3 in figure 4.10, we can see that the reactive power demand of the wind farm increases again from around 100 s and this increase in demand continues until the voltage collapses. Exactly what causes the wind farm to consume the very large amounts of reactive power leading up to the voltage collapse has not been determined. In figure 4.11(d), we can also see how the LTC transformers re-initiate their operation in an attempt to restore the voltage at around 110 s.

Figure 4.11(e) shows how this increase in reactive power demand causes the activation of additional current limiters. Eventually, the grid cannot cope with this increased demand and the voltage eventually collapses at around 155 s.

This increased demand of reactive power following the simulated contingency, enhanced by the asynchronous nature of the wind farm, is one factor that drives the system

to collapse. It makes sense to install additional reactive power support to help the system cope with this increased demand. In the following section we are going to investigate how adding an SVC affects the stability of the power system.

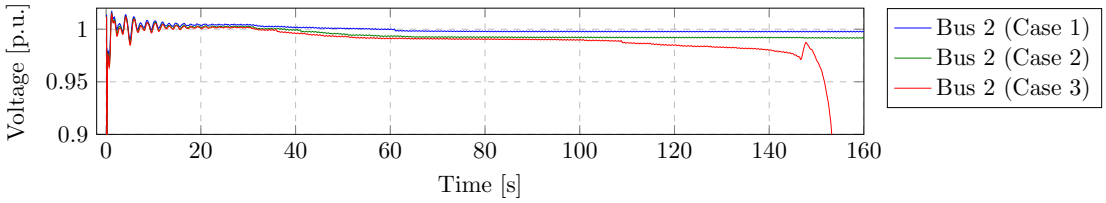

(a) Voltage profiles of bus 16 for three different transfer cases.

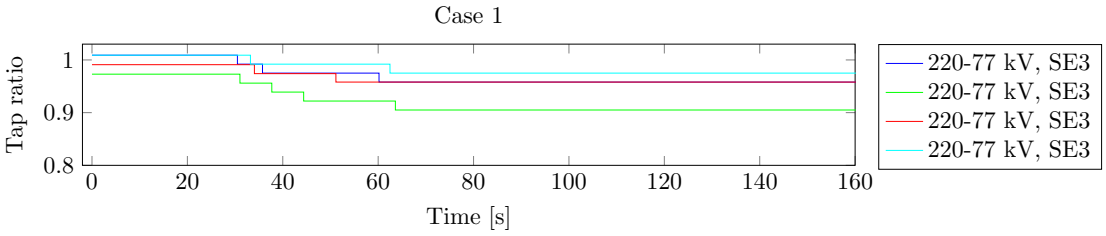

(b) LTC operation of three SE3 transformers for transfer case 1.

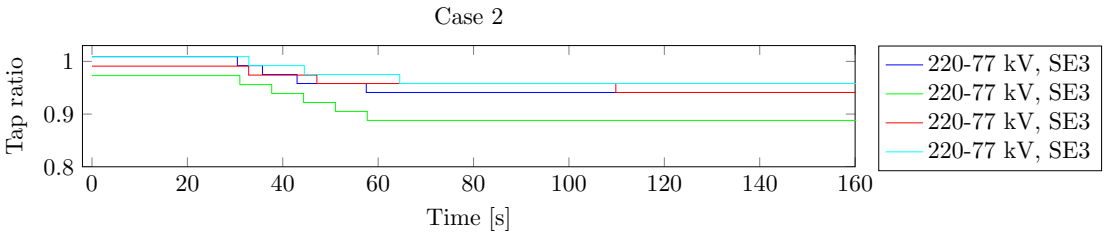

(c) LTC operation of three SE3 transformers for transfer case 2.

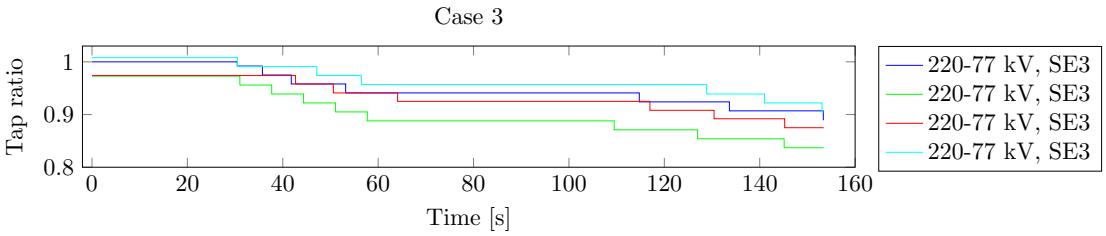

(d) LTC operation of three SE3 transformers for transfer case 3.

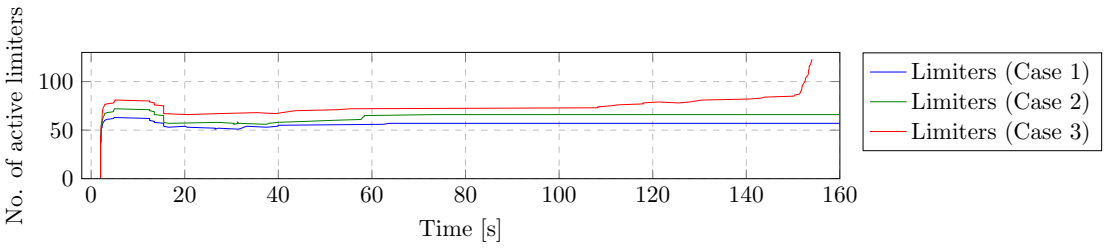

(e) Number of active generator current limiters for three different transfer cases.

Figure 4.11: Voltage profiles, LTC operation and number of active generator current limiters for three different transfer cases where a large, induction generator based wind farm has been added to the system.

Adding an SVC to increase the interface capacity

To determine the most suitable SVC location, the $VCPI$ index is calculated for the load flow case including the wind farm. In this case, only the $VCPI$ index is considered to reduce the number of simulations.

Figure 4.12 shows a bar chart of the calculation result. A complete list of the calculated $VCPI$ indices is presented in appendix B. Table 4.12 lists the five highest

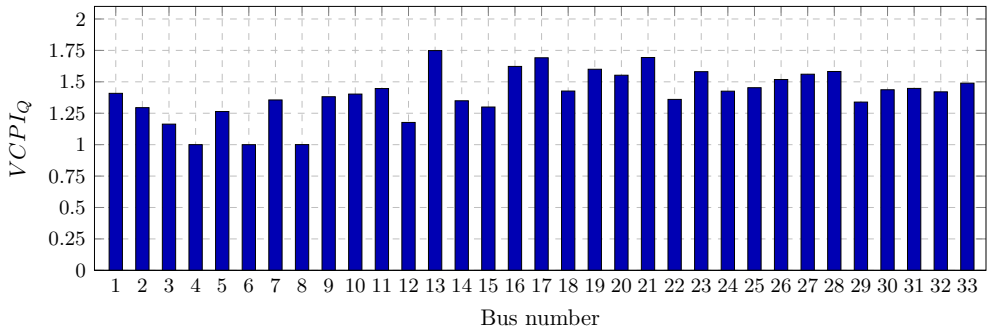

Figure 4.12: $VCPI$ indices for the case with an added wind farm modelled by CIMTR3.

ranked buses based on the $VCPI$ index. Bus 13 is the highest ranked bus for this transfer case and this is also the wind farm connection bus. Bus 13 is therefore chosen for the installation of an SVC. To evaluate how it affects the interface capacity, a ±200 MVAr SVC is installed to bus 13.

Table 4.12: The five buses with the highest $VCPI$ index for the case with an added, induction generator modeled, wind farm.

Rank	Bus no.	$VCPI_Q$
1.	13	1.748
2.	21	1.693
3.	17	1.691
4.	16	1.622
5.	19	1.600

By adding the SVC, the interface transfer capacity is increased to 7850 MW. The capacity is thus increased by 1000 MW, a substantial change compared to the previous results in section 4.4.3.

Comparing SVC and switched shunt compensation

For completeness, it is interesting to compare the results from the SVC installation to the corresponding results from installing regular switched shunt compensation.

The SVC in the previous simulations is replaced by a switched shunt installation with the same power rating, i.e. ±200 MVAr. By performing the same set of simulations as before, the highest stable interface transmission with switched shunt compensation was determined to 7350 MW. Table 4.13 lists how the interface capacity is affected by adding either an SVC or switched shunt compensation.

If the SE2-SE3 transmission is increased, a problem with short-time voltage stability is eventually introduced. This instability follows from the simulation of contingency 14 and it causes the system to suffer a voltage collapse within a few seconds.

Table 4.13: Comparison of SVC and switched shunt compensation.

Case	Interface capacity [MW]	Capacity increase [MW]
No compensation	6850	-
SVC	7850	1000
Switched shunts	7350	500

This transient problem is shown in figure 4.13, where the SE2-SE3 interface transmission is equal to 7850 MW.

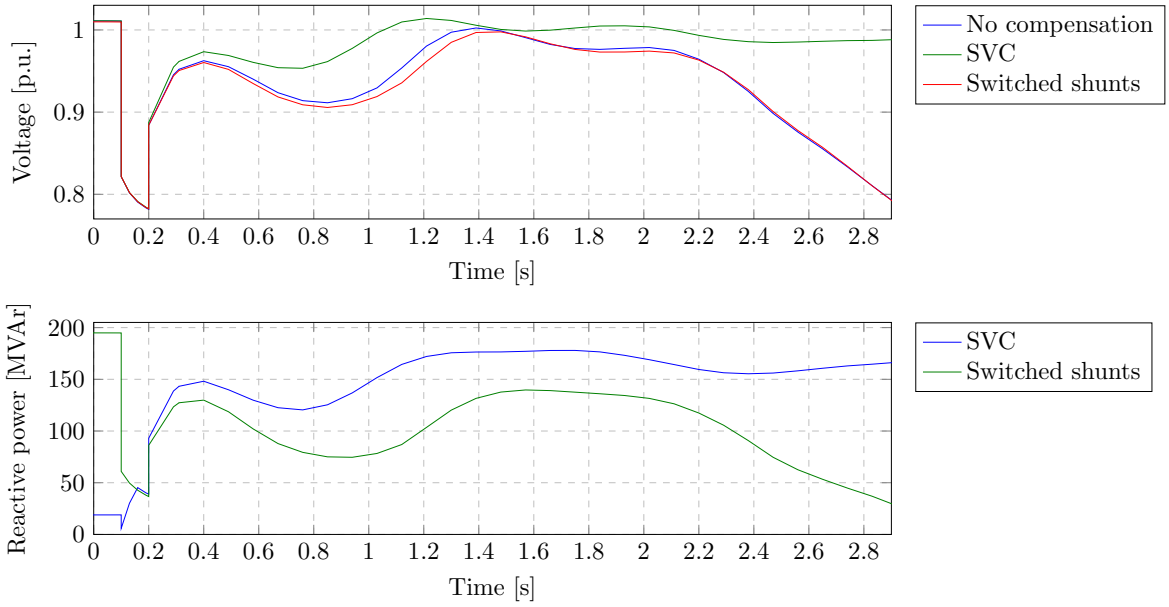

Figure 4.13: Voltage profiles at bus 2 and reactive power injection at bus 13. Contingency 14 is applied at $t = 0$ s and cleared after 100 ms when the faulted line also is disconnected.

Note that the reactive power injected by the SVC is increased as soon as the line is disconnected at $t = 0.1$ s. This fast reactive power response is enough to bring the system into a stable state of operation.

In the uncompensated case, this instability presents itself when the interface transfer exceeds 7300 MW. Adding an SVC to the wind farm connection greatly enhances stability by solving the voltage collapse presented in figure 4.10 and it also solves the short-time voltage problem presented in figure 4.13. Using regular switched shunt compensation increases the stability of the system to some extent, but it is not as effective as the SVC.

These simulation results illustrate how the fast response time of the SVC can be used to effectively improve both the long-term and short-time voltage stability of power systems.

4.5.2 Wind farm based on doubly fed induction generators (DFIGs)

This section focuses on the investigation of how a wind farm based on doubly fed induction generators (DFIGs) would affect the power system. The wind power generators are modeled using the set of wind power models included in PSS™E [49].

The wind turbine generator (WTG) model used in this thesis is General Electric (GE) 3.6 MW, 50 Hz. This WTG model comprises a number of models for aerodynamics, the generator, control and protection systems. See appendix C for the complete list of used models and parameters.

In the simulations, the wind farm is modeled by aggregating 278 generators on a dummy bus connected to bus 13 in the high voltage transmission grid through a lossless line. The total power of the wind farm is thus 1000.8 MW.

When initiating the wind generator model in PSS^{TM}E, a number of parameters are set to define the operation of the wind farm. The dispatch mode of the wind farm was set to *dispatch directly*, at 98% of the total power and the control option was set to *power factor control*. By using power factor control, the reactive power exchange between the wind farm and the grid is set to zero. Additionally, a set of protective schemes are added to the modeled wind farm. In these simulations a voltage and a frequency protection scheme are added to the generator bus. All of these parameters are set because they are all required to meet the requirements today.

The simulations follow the same methodology as described for the induction generator based wind farm described earlier in section 4.5.1. Table 4.14 lists the interface transfer for three cases used in the simulations.

Table 4.14: The simulated cases and their level of transfer across SE2-SE3.

Case description	SE2-SE3 transfer [MW]
Case 1	8150
Case 2	8350
Case 3	8400

Figure 4.14 shows the voltage profile of bus 2 when contingency 14 has been applied to each of the cases. Here we can see that the highest stable transfer is determined for case 2 at 8350 MW.

Comparing the SE2-SE3 transfer capacity for the two different wind farm simulations in tables 4.10 and 4.14 we note a 1500 MW higher capacity for the DFIG based wind farm. The DFIG wind farm represents a more modern technology, equipped with the various control and protection systems mentioned earlier. These added control systems leads to a more stable power system compared to the case with the induction generator based wind farm which lacked these systems.

The transfer capacity of the SE2-SE3 interface is therefore higher when basing the wind farm on DFIGs (compared to the previous, induction generator case).

Case 3 is considered unstable as it enters one of the unacceptable operating situations mentioned earlier in section 4.1.1. The voltage of a 400 kV bus (not bus 2 however), is below 0.875 p.u. for 5 s and the simulation is thus terminated.

The jump in voltage level at about 45 s for case 1 in figure 4.14 is again caused by the activation of the emergency protection system. Note that, in these simulations, the wind farm does not increase its reactive power demand as the voltage level is lowered as we saw previously in figure 4.10. The protection and control schemes added to the DFIG based wind farm prevents the behaviors seen for the induction generator based wind farm in section 4.5.1. This indicates that the voltage problem in case 3 is not caused by the wind farm's reaction to the applied contingency.

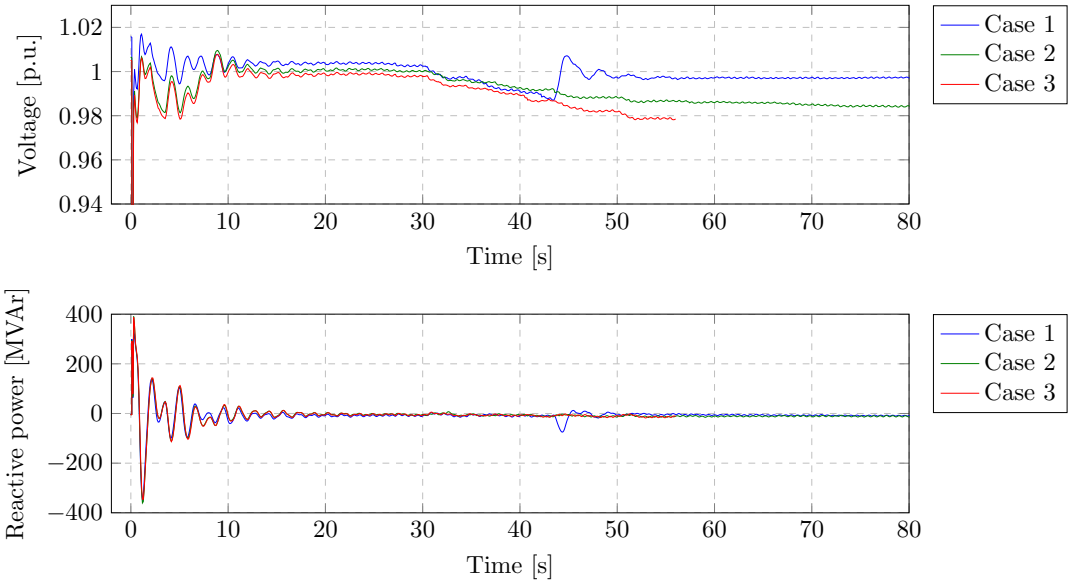

Figure 4.14: Voltage profiles of bus 2 and reactive power exchange for the wind farm based on DFIGs.

Adding an SVC to increase the interface capacity

This section investigates how the interface capacity could be increased by installing an additional SVC. The methodology for this study is the same as described before in section 4.5.1. Figure 4.15 presents the $VCPI$ indices for the studied buses when a DFIG based wind farm has been added to the grid. Caculations of the $VCPI$ indices are based on the transfer case "$VCPI_Q$ GEWIND" listed in appendix A.

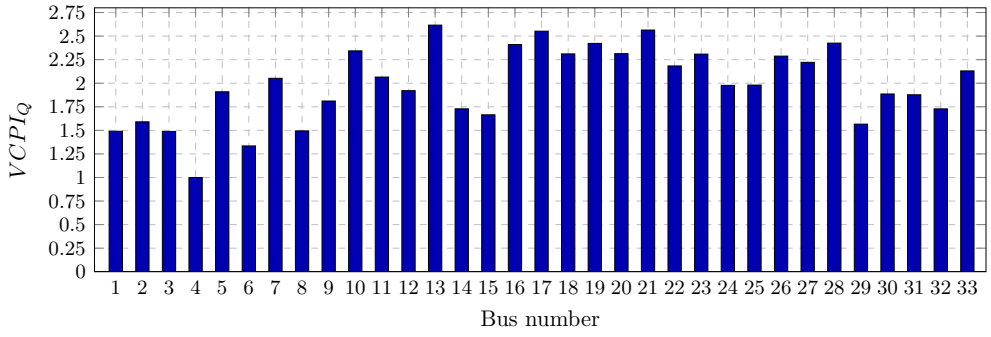

Figure 4.15: $VCPI$ indices for the studied buses where a DFIG based wind farm has been added to the grid.

Table 4.15 lists the 5 buses with the highest $VCPI$ value. The complete list is presented in appendix B. Bus 13 is used as the candidate bus for an additional SVC installation as it is the highest ranked bus.

Adding a ±200 MVAr SVC to bus 13 increases the interface transfer capacity to 8450 MW. Comparing to the highest stable case without additional compensation (Case 2) we can conclude that adding an SVC to bus 13 increases the SE2-SE3 capacity by 100 MW.

Table 4.15: The five buses with the highest $VCPI$ index for the case with an added, DFIG modeled, wind farm.

Rank	Bus no.	$VCPI_Q$
1.	13	2.616
2.	21	2.564
3.	17	2.552
4.	28	2.426
5.	19	2.423

The addition of an SVC to the connection bus of a DFIG based wind farm has only a rather small impact on the transfer capacity of the SE2-SE3 interface. This result is not very surprising as the reactive power demand of the wind farm is close to zero after the oscillations in figure 4.14 have ended.

Comparing these results to those from the simulations of the induction generator based wind farm in figure 4.10, we can see how the reactive power demand of that wind farm is gradually increased when the voltage level is decreased. This is why the SVC has a much greater impact for the induction generator based wind farm.

Comparing SVC and switched shunt compensation

To complete the study of the DFIG based wind farm, simulations are performed for the case where the SVC is replaced by switched shunt compensation. The switched shunt has the same rating as the SVC, i.e. ±200 MVAr.

The same set of simulations has been performed as with the SVC earlier and the highest interface capacity using the switched shunt was determined to 8450 MW, i.e. the same as in the SVC compensated case. An increase in interface capacity equal to 100 MW. Table 4.16 presents a summary of the results from these simulations.

Table 4.16: Comparison of SVC and switched shunt compensation for the DFIG based wind farm.

Case	Interface capacity [MW]	Capacity increase [MW]
No compensation	8350	-
SVC	8450	100
Switched shunt	8450	100

Compare this increase in interface capacity to the case without any additional reactive power support listed in table 4.14. It can be seen that adding either an SVC or a switched shunt to the bus connecting a DFIG based wind farm will not yield the same effect as we saw earlier in the case with the induction generator based wind farm.

Based on these results we can conclude that in this case, adding an SVC to the connection bus of a DFIG based wind farm will not be more useful than a regular switched shunt.

4.6 Study of the socio-economic benefits

This section presents an electricity market study, performed to evaluate the socio-economic benefits, or rather the electricity market benefits, associated with increasing the transfer capacity of the SE2-SE3 interface. The study is performed by using version 2.4 of the electricity market model "Better Investment Decisions (BID)", developed by Pöyry.

The BID model is an electricity market model that covers the Nordic region, Netherlands, Belgium, UK, France, Germany, Poland, Switzerland, Austria and the Baltic countries [50]. It assumes perfect competition and models both thermal and hydro power plants. Note that BID is only able to model the electricity market and does not support calculations coupled with power system calculations such as load-flow.

In this thesis, the electricity market model used for our calculations is an estimate of the market as of 2015. This is the model which corresponds most accurately to the 2007 Nordic power grid used in previous simulations. Note that this is the oldest market model used at Svenska Kraftnät at the time this was written.

To evaluate how the increased transfer capacity of the SE2-SE3 interface would benefit the electricity market of the modeled countries mentioned above, three different cases are prepared. These cases are modeled with different NTC values of the SE2-SE3 interface based on the results presented in section 4.4.3. The SE2-SE3 NTC is thus increased by 100, 150 and 200 MW respectively.

In this study, the market simulations are based on three different scenarios to represent the yearly variations in water level. The three scenarios are

- Normal year - based on hydro data from 1998
- Dry year - based on hydro data from 1996
- Wet year - based on hydro data from 2000

where all three scenarios share the same wind data from 2009.
Table 4.17 and figure 4.16 presents the simulation results for the different scenarios and the different interface increases.

Table 4.17: Electricity market benefit for the different scenarios and interface increases.

Increased interface capacity [MW]	Dry year [M€/year]	Normal year [M€/year]	Wet year [M€/year]
100	-1.5	-1.3	-0.4
150	-0.9	-1.9	-3.2
200	0.1	-2.4	9.6

The market simulations performed in this section are only based on electricity prices throughout the european market. As we study the impact on the system by increasing the transfer capacity of the SE2-SE3 interface, we are thus interested in how this increase would affect the electricity prices. In order to achieve a large market benefit, the electricity prices would have to be lowered by allowing more, cheap hydro power to be transferred south from northern Scandinavia.

The results from this study of the modeled european electricity market indicates that increasing the capacity of the SE2-SE3 interface, by up to 200 MW, does not yield much market benefit. As we can see in figure 4.16, the increased yearly market benefit

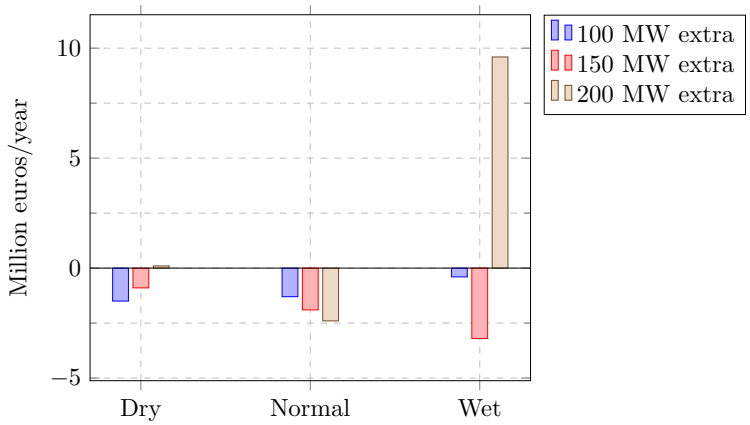

Figure 4.16: Increased yearly benefit of the european electricity market for the simulated scenarios.

of the simulated cases are quite small. These results are actually small enough to be within the uncertainties of the calculations [51].

Installing an additional ±200 MVAr SVC would cost close to 15.5 M€, whilst an additional 200 MVAr switched shunt capacitor would cost around 1.4 M€. The cost of installing any of these components would have to be motivated by other system benefits rather than electricity market benefits.

Chapter 5

Conclusions and future work

In this final chapter of the thesis we discuss the results from the performed simulation study. We also discuss and suggest further work within this area.

5.1 Conclusions

This thesis has examined the concept of voltage stability and methods used to evaluate and extend the stability limits of a power system. The work has been focused on SVCs and how they could be used to stabilize the power system to avert a voltage collapse situation.

Sensitivity indices have been presented and evaluated to identify areas in the Swedish power system which are prone to suffer a voltage collapse under certain stressed conditions. It has been determined that the implementation of additional reactive power compensation in these weaker areas of the grid could increase power transfer capability of the SE2-SE3 interface.

Simulations of the 2007 Nordic power system showed that both the $VCPI$ and the Q-V sensitivity index identified the same area in SE3 as weak and prone to suffer a voltage collapse. However, when adding an SVC to the buses ranked as weakest by the two indices, the $VCPI$ gave the slightly better results.

The Q-V sensitivity index did not rank the weak buses in the same order as the $VCPI$ and this could have been caused by having to perform the Q-V simulations with locked transformer taps. This surely affected the simulation results, but both indices still pointed to the same weak area of the grid. Based on these results we conclude that in this case, the Q-V sensitivity index is more suited for preliminary studies. To yield more accurate results however, additional simulations are needed to verify which buses that are the weakest. This thesis has shown that the $VCPI$ can be a useful tool for these additional studies.

Table 5.1 lists the best results from the simulation study based on the Nordic power system as it existed in 2007. Installing an additional SVC to the studied power system

Table 5.1: Largest interface increase for different types of compensation.

Type of compensation	Rating [MVAr]	Interface increase [MW]
SVC	±200	150
SVC	±400	200
Switched shunts	±200	100

could increase the interface capacity up to 200 MW. It is interesting to compare the increase in transmission capacity achieved by regular switched shunt compensation rated the same as one of the studied SVCs. In this case it was shown that the SVC provided an additional increase in capacity equal to 50 MW.

When a large, induction generator based wind farm was added to a weak area of the power system, the benefits of installing an SVC became much more pronounced. In this simulated case, the interface transfer was limited by the introduction of a transient problem. By installing an SVC to the wind farm connection bus it was possible to increase the interface capacity by 1000 MW. Using regular switched shunt compensation with an equal power rating did only enable a capacity increase equal to 500 MW.

Simulations were also performed with an added DFIG based wind farm of the same size as the induction generator based farm. In this case we could not see the same benefit from adding additional compensation to the wind farm connection. Adding a ±200 MVAr SVC at the wind farm connection bus would increase the interface capacity by 100 MW. We could also see the same capacity increase if switched shunts were used instead of the SVC.

Table 5.2 lists the results from the simulation study with the added wind farms, where the CIMTR3 model was used for the induction generator based wind farm.

Table 5.2: Largest interface increase for different types of compensation.

Compensation type	Wind farm model	Rating [MVAr]	Interface increase [MW]
SVC	CIMTR3	±200	1000
Switched shunt	CIMTR3	±200	500
SVC	DFIG	±200	100
Switched shunt	DFIG	±200	100

Based on the simulation study performed in this thesis, it can be concluded that additional SVCs can increase the interface capacity substantially. We could see the greatest impact when an SVC was installed at the connection of an induction generator based wind farm in a weak area of the grid. In this case, with a transient problem as the limiting factor, the SVC clearly outperformed the regular shunt compensation.

However, SVCs are not to be considered a general solution for increasing transfer capacity. This thesis has shown that if an SVC was installed to the 2007 Nordic power system, it would only give a 50 MW capacity increase compared to the much cheaper regular switched shunt capacitor. Additionally, in the case with a DFIG based wind farm in a weak area, the SVC and switched shunt compensation performed equally. Both devices enabled an interface increase of 100 MW.

These results suggest that certain power systems could benefit a lot from additional SVCs. Grids limited by transient problems, weaker grids (e.g. grids with a pronounced radial structure [52,53]) or power grids with a large wind power penetration are examples of power systems where an SVC could prove very useful.

Finally, a last conclusion may be drawn. An SVC can be a very effective device for voltage control and can be used to improve the power transfer across congested interfaces. However, thorough studies are needed to determine the actual benefit of this rather expensive device as some grids may receive equal benefits by using regular switched shunt compensation.

5.2 Future work

This thesis has only focused on how an SVC could improve the transfer capacity of interface SE2-SE3. However, the FACTS family of devices comprises additional interesting power electronic based components.

In future studies it would be interesting to investigate how the interface capacity would be affected by either of these FACTS components:

- Static synchronous compensator (STATCOM)
- Thyristor controls series capacitor (TCSC)
- United power flow controller (UPFC)

This should not pose a very big challenge as PSS™E already includes built-in models for each of these components.

It would also be interesting to investigate how the placement strategies could be based on alternative techniques such as:

- Optimal power flow (OPF)
- Eigenvalue based techniques

As PSS™E can handle these methods by installing extra toolboxes, it is quite possible to investigate these methods.

This thesis has been based on the Nordic power grid as it existed in 2007. Future simulations should be performed on a more recent power system model to evaluate how the proposed methods would apply.

Appendix A

Transfer data

Table A.1: Detailed transfer data for the different cases, all transfer data presented in MW.

Area	Base case	Case 1	Case 2	Case 3	Case 4
SE1–NO4	131	-243	-243	-243	-263
SE1–FI	560	506	506	506	504
SE1–SE2	1711	2678	2726	2725	2794
SE2–NO4	2	-149	-152	-152	-162
SE2–NO3	241	-120	-132	-132	-170
SE2–SE3	**5728**	**8514**	**8616**	**8662**	**8717**
SE3–NO1	-375	-697	-709	-711	-740
SE3–FI	-536	-536	-536	-536	-536
SE3–DK	0	0	0	0	0
SE3–SE4	2681	2732	2730	2731	2732
SE4–DK2	33	33	33	33	33
SE4–PL	-200	-200	-200	-200	-200
SE4–DE	-400	-400	-400	-400	-400

Table A.2: Detailed transfer data for the different cases with added wind farm, all transfer data presented in MW.

Area	Case 1	Case 2	Case 3
SE1–NO4	22	24	23
SE1–FI	521	522	521
SE1–SE2	2310	2309	2310
SE2–NO4	-25	-23	-21
SE2–NO3	214	216	217
SE2–SE3	**6701**	**6854**	**6907**
SE3–NO1	-437	-442	-444
SE3–FI	-536	-536	-536
SE3–DK	0	0	0
SE3–SE4	2712	2715	2716
SE4–DK2	33	33	33
SE4–PL	-200	-200	-200
SE4–DE	-400	-400	-400

Table A.3: Detailed transfer data for the different cases used to calculate the $VCPI$ indices.

Area	$VCPI_Q$	$VCPI_Q$ CIMTR3	$VCPI_Q$ GEWIND
SE1–NO4	-271	24	-152
SE1–FI	503	522	514
SE1–SE2	2804	2309	2684
SE2–NO4	-164	-23	-123
SE2–NO3	-173	216	-46
SE2–SE3	**8597**	**6853**	**8263**
SE3–NO1	-735	-441	-660
SE3–FI	-536	-536	-536
SE3–DK	0	0	0
SE3–SE4	2730	2714	2740
SE4–DK2	33	33	33
SE4–PL	-200	-200	-200
SE4–DE	-400	-400	-400

Appendix B

List of calculated indices

B.1 Q-V sensitivity

Table B.1: Q-V sensitivities for the investigated buses.

Bus no.	Area	Slope [MVAr/p.u. voltage]
1.	2	4 474
2.	2	15 182
3.	2	4 101
4.	2	Slack bus
5.	2	5 738
6.	2	18 549
7.	2	5 298
8.	2	14 230
9.	2	6 691
10.	3	7 010
11.	3	7 725
12.	3	4 771
13.	3	9 101
14.	3	8 285
15.	3	7 587
16.	3	13 565
17.	3	14 884
18.	3	8 667
19.	3	18 864
20.	3	15 576
21.	3	13 344
22.	3	5 333
23.	3	19 664
24.	3	4 742
25.	3	8 402
26.	3	11 204
27.	3	5 170
28.	3	9 054
29.	3	9 870
30.	3	12 488
31.	3	11 617
32.	3	10 807
33.	3	——

B.2 $VCPI$ index

Table B.2: $VCPI_Q$ list for the investigated buses.

Bus no.	Area	$VCPI_Q$	$VCPI_Q$ CIMTR3	$VCPI_Q$ GEWIND
1	2	1.937	1.408	1.490
2	2	1.737	1.295	1.591
3	2	1.499	1.163	1.489
4	2	1.000	1.000	1.000
5	2	1.908	1.264	1.909
6	2	1.337	1.000	1.335
7	2	2.024	1.356	2.052
8	2	1.495	1.001	1.494
9	2	1.932	1.381	1.811
10	3	2.302	1.402	2.343
11	3	2.017	1.447	2.065
12	3	1.893	1.177	1.921
13	3	2.429	1.748	2.617
14	3	1.649	1.349	1.729
15	3	1.678	1.300	1.665
16	3	2.268	1.622	2.411
17	3	2.410	1.691	2.552
18	3	2.251	1.427	2.311
19	3	2.376	1.600	2.423
20	3	2.189	1.553	2.314
21	3	2.420	1.693	2.564
22	3	2.172	1.360	2.183
23	3	2.220	1.581	2.309
24	3	1.922	1.426	1.977
25	3	2.078	1.453	1.981
26	3	2.200	1.518	2.288
27	3	2.056	1.561	2.222
28	3	2.325	1.582	2.426
29	3	1.512	1.339	1.566
30	3	1.823	1.437	1.886
31	3	1.813	1.448	1.877
32	3	1.671	1.420	1.728
33	3	2.019	1.490	2.131

Appendix C

Wind model parameters

C.1 CIMTR3

Table C.1: Static load flow representation of the induction generator used to model the induction generator based wind farm.

Parameter	Minimum value	Maximum value
Active power, P	0.0 MW	90.18 MW
Reactive power, Q	-24.55 MVAr	-24.55 MVAr

Table C.2: List of the parameters used in the dynamic model CIMTR3.

Parameter	Value	Unit
T'	0.6904	(sec)
T''	0.0	(sec)
H	4.0	(p.u.)
X	3.7959	(p.u.)
X'	0.1921	(p.u.)
X''	0.0	(p.u.)
X_1	0.0745	(p.u.)
E_1	1.0	(p.u.)
$S(E_1)$	0.2093	
E_2	1.1	(p.u.)
$S(E_2)$	0.4694	
Switch	0	
SYN-POW	0.01	

C.2 GE 3.6 MW, 50 Hz

Table C.3: Model: GECNA

Parameter	Value	Unit
PFAFLG	1	
VARFLG	0	
T_{fv}	0.15	s
K_{pv}	18.0	p.u.
K_{iv}	5	p.u.
R_c	0	p.u.
X_c	0	p.u.
T_{fp}	0.05	s
K_{pp}	3	p.u.
K_{ip}	0.6	p.u.
P_{max}	1.12	p.u.
P_{min}	0.1	p.u.
Q_{max}	0.52	p.u.
Q_{min}	-0.39	p.u.
IP_{max}	1.11	p.u.
T_{rv}	0.05	s
RPMX	0.45	p.u.
RPMN	-0.45	p.u.
T_{power}	5	s
K_{Qi}	0.5	Volt/MVAr gain
V_{min}	0.9	p.u.
V_{max}	1.1	p.u.
K_{Vi}	40	p.u.
XI_{Qmin}	-0.5	p.u.
XI_{Qmax}	0.4	p.u.
T_V	0.05	s
T_P	0.05	s
F_n	1	

Table C.4: Model: GEAERA

Parameter	Value	Unit
λ_{max}	20	
λ_{min}	0	
PITCH_{max}	27	
PITCH_{min}	-4	
T_a	0	
ρ	1.225	kg/m^3
Radius	52	m
GB_{ratio}	117.5	
Synchr	1500	rpm
Power_Rate	3600	kW
MBASE1	4.0	MVA

Table C.5: Turbine data

Parameter	Value	Unit
Base voltage	3.3	kV
WTG MBASE	4.0	MVA
Transformer MBASE	4.0	MVA
Transformer R	0	p.u.
Transformer X	0.07	p.u.
GTAP	1.0	
P_{max}	3.6	MW
P_{min}	0.5	MW
X_{eq}	0.8	p.u.
L_A	0.17	p.u.
L_M	2.66	p.u.
R_1	0.0047	p.u.
L_1	0.1	p.u.
Inertia	1.277	
Damping	0	
Q_{max}	2.0	MVAr
Q_{min}	-1.55	MVAr

Table C.6: Model: GEDFA

Parameter	Value	Unit
TI_{pcmd}	0.02	s
TE_{pcmd}	0.02	s
K_{PLL}	30	p.u.
PLL_{max}	0.1	
PLL_{min}	-0.1	

Table C.7: Model: WGUSTA

Parameter	Value	Unit
$T1_g$	9999	s
T_g	5	s
MAXG	30	m/s
$T1_r$	9999	s
$T2_r$	9999	s
MAXR	30	m/s

Table C.8: Model: W2MSFA

Parameter	Value	Unit
D12	2.1	p.u.
K12	3.56	p.u.
Ta1	6.79	s
POL	2	
R_q	117.5	

Table C.9: Model: GEPCHA

Parameter	Value	Unit
T_p	0.3	s
K_{ppt}	150	p.u.
K_{ipt}	25	p.u.
K_{pc}	3.33	p.u.
K_{ic}	33.3	p.u.
θ_{min}	-4	degrees
θ_{max}	27	degrees
$d\theta/dt_{min}$	-10	degrees/s
$d\theta/dt_{max}$	10	degrees/s
P_{ref}	0.9	

Table C.10: Voltage and frequency protection parameters.

Parameter	Value	Unit	Parameter	Value	Unit
$V_{low}(1)$	0.15	p.u.	$F_{low}(1)$	47.0	Hz
$V_{low}(2)$	0.50	p.u.	$F_{low}(2)$	47.5	Hz
$V_{low}(3)$	0.90	p.u.	$F_{up}(1)$	51.25	Hz
$V_{up}(1)$	1.10	p.u.	$F_{up}(2)$	52.0	Hz
$V_{up}(2)$	1.15	p.u.	$V_{pickup\ time}(1)$	0.02	s
$V_{up}(3)$	1.30	p.u.	$V_{pickup\ time}(2)$	10.0	s
$V_{pickup\ time}(1)$	0.01	s	$V_{pickup\ time}(3)$	30.0	s
$V_{pickup\ time}(2)$	1.3	s	$V_{pickup\ time}(4)$	0.02	s
$V_{pickup\ time}(3)$	3.0	s	$V_{breaker\ time}$	0.08	s
$V_{pickup\ time}(4)$	3.0	s			
$V_{pickup\ time}(5)$	1.3	s			
$V_{pickup\ time}(6)$	0.01	s			
$V_{breaker\ time}$	0.08	s			

Bibliography

[1] S. Larsson and A. Danell, "The black-out in southern Sweden and eastern Denmark, September 23, 2003," in *Power Systems Conference and Exposition, 2006. PSCE '06. IEEE PES*, Oct. 29–Nov. 1 2006, pp. 309–313.

[2] U.S.-Canada Power System Outage Task Force, "Final report on the august 14, 2003 blackout in the United States and Canada: Causes and recommendations," U.S. Department of Energy and Natural Resources Canada, Tech. Rep., Apr. 2004. [Online]. Available: https://reports.energy.gov/BlackoutFinal-Web.pdf

[3] S. Corsi and C. Sabelli, "General blackout in italy sunday september 28, 2003, h. 03:28:00," in *2004. IEEE Power Engineering Society General Meeting*, Jun.10 2004, pp. 1691–1702 Vol. 2.

[4] I. C. Decker, M. N. Agostini, A. S. e Silva, and D. Dotta, "Monitoring of a large scale event in the Brazilian power system by WAMS," in *2010 iREP Symposium Bulk Power System Dynamics and Control – VIII (iREP)*, Aug.1-6 2010, pp. 1–8.

[5] The enquiry committee, "Grid disturbance in northern region on 30th july 2012 and in northern, eastern & north-eastern region on 31st july 2012," Aug. 2012. [Online]. Available: http://www.powermin.nic.in/pdf/GRID_ENQ_REP_16_8_12.pdf

[6] G. Andersson, P. Donalek, R. Farmer, N. Hatziargyriou, I. Kamwa, P. Kundur, N. Martins, J. Paserba, P. Pourbeik, J. Sanchez-Gasca, R. Schulz, A. Stankovic, C. Taylor, and V. Vittal, "Causes of the 2003 major grid blackouts in North America and Europe, and recommended means to improve system dynamic performance," *IEEE Transactions on Power Systems*, vol. 20, no. 4, pp. 1922–1928, Nov. 2005.

[7] C. W. Taylor, *Power System Voltage Stability*. McGraw-Hill, 1994.

[8] P. Kundur, *Power System Stability and Control*. McGraw-Hill, 1994.

[9] P. Kundur, J. Paserba, V. Ajjarapu, G. Andersson, A. Bose, C. Canzares, N. Hatziargyriou, D. Hill, A. Stankovic, C. Taylor, T. Van Cutsem, and V. Vittal, "Definition and classification of power system stability IEEE/CIGRE joint task force on stability terms and definitions," *IEEE transactions on Power Systems*, vol. 19, no. 3, pp. 1387–1401, Aug. 2004.

[10] T. Van Cutsem, "Voltage instability: Phenomena, countermeasures, and analysis methods," *Proceedings of the IEEE*, vol. 88, no. 2, pp. 208–227, Feb. 2000.

[11] J. Dixon, L. Morán, J. Rodríguez, and R. Domke, "Reactive power compensation technologies: State-of-the-art review," *Proceedings of the IEEE*, vol. 93, no. 12, pp. 2144–2164, Dec. 2005.

[12] N. Hingorani, "Flexible ac transmission," *Spectrum, IEEE*, vol. 30, no. 4, pp. 40–45, 1993.

[13] L. Gyugyi, "Reactive power generation and control by thyristor circuits," *IEEE Transactions on Industry Applications*, vol. IA-15, no. 5, pp. 521–532, Sep. 1979.

[14] R. Boyer, R. ElFakir, D. Larsson, and T. Rosenberger, "Dallas fort worth svc project: Parkdale svc," in *Power Energy Society General Meeting, 2009. PES '09. IEEE*, 2009, pp. 1–8.

[15] D. L. Dickmander, B. H. Thorvaldsson, G. A. Strömberg, D. L. Osborn, A. E. Poltras, and D. A. Fisher, "Control system design and performance verification for the Chester, Maine static VAr compensator," *IEEE transactions on Power Delivery*, vol. 7, no. 3, pp. 1492–1503, Jul. 1992.

[16] D. Sullivan, J. Paserba, G. Reed, T. Croasdaile, R. Westover, R. Pape, M. Takeda, S. Yasuda, H. Teramoto, Y. Kono, K. ichi Kuroda, K. Temma, W. Hall, D. Mahoney, D. Miller, and P. Henry, "Voltage control in southwest utahwith the st. george static var system," in *Power Systems Conference and Exposition, 2006. PSCE '06. 2006 IEEE PES*, 2006, pp. 459–465.

[17] G. Vukojevic, A. Svalovs, K. A. S. Ghadem, and A. O. D. Ali, "Transient analysis of svc response in the south region of the Libyan transmission network," in *PowerTech, 2011 IEEE Trondheim*, Jun.19-23 2011, pp. 1–6.

[18] J. Kowalski, I. Vancers, M. Reynolds, and H. Tyll, "Application of static var compensation on the southern california edison system to improve transmission system capacity and address voltage stability issues - part 1. planning, design and performance criteria considerations," in *Power Systems Conference and Exposition, 2006. PSCE '06. 2006 IEEE PES*, Oct. 30–Nov. 2 2006, pp. 451–458.

[19] E.-Z. Zhou, "Application of static var compensators to increase power system damping," *Power Systems, IEEE Transactions on*, vol. 8, no. 2, pp. 655–661, May 1993.

[20] Y.-L. Chen, "Weak bus-oriented optimal multi-objective var planning," *IEEE Transactions on Power Systems*, vol. 11, no. 4, pp. 1885–1890, Nov. 1996.

[21] B. Gao, G.K. Morison, and P. Kundur, "Voltage stability evaluation using modal analysis," *IEEE Transactions on Power Systems*, vol. 7, no. 4, pp. 1529–1542, Nov. 1992.

[22] P.-A. Löf, T. Smed, G. Andersson, and D. J. Hill, "Fast calculation of a voltage stability index," *IEEE Transactions on Power Systems*, vol. 7, no. 1, pp. 54–64, Feb. 1992.

[23] C. A. Cañizares, A. C. Z. de Souza, and V. H. Quintana, "Comparison of performance indices for detection of proximity to voltage collapse," *IEEE Transactions on Power Systems*, vol. 11, no. 3, pp. 1441–1450, Aug. 1996.

[24] V. Ajjarapu and C. Christy, "The continuation power flow: a tool for steady state voltage stability analysis," *IEEE Transactions on Power Systems*, vol. 7, no. 1, pp. 416–423, Feb. 1992.

[25] Y.-L. Chen, C.-W. Chang, and C.-C. Liu, "Efficient methods for identifying weak nodes in electrical power networks," *IEE Proceedings-Generation, Transmission and Distribution*, vol. 142, no. 3, pp. 317–322, May 1995.

[26] T. Van Cutsem and C. Vournas, *Voltage Stability of Electric Power Systems*. Springer Science+Business Media, LLC, 2008.

[27] IEEE Task Force on Load Representation for Dynamic Performance, "Load representation for dynamic performance analysis," *IEEE transactions on Power Systems*, vol. 8, no. 2, pp. 472–482, May 1993.

[28] V. Ajjarapu, *Computational Techniques for Voltage Stability Assessment and Control*. Springer, 2006.

[29] S. Torseng, "Shunt-connected reactors and capacitors controlled by thyristors," *IEE Proceedings C Generation, Transmission and Distribution*, vol. 128, no. 6, pp. 366–373, Nov. 1981.

[30] Å. Ölwegård, K. Walve, G. Wåglund, H. Frank, and S. Torseng, "Improvement of transmission capacity by thyristor controlled reactive power," *IEEE Transactions on Power Apparatus and Systems*, vol. PAS-100, no. 8, pp. 3930–3939, Aug. 1981.

[31] *IEEE Guide for the Functional Specification of Transmission Static Var Compensators*, IEEE Std. 1031, Jun. 2011.

[32] N. Mohan, T. M. Undeland, and W. P. Robbins, *Power Electronics: Converters, Applications and Design*, 3rd ed. John Wiley & Sons, Mar. 2003.

[33] M. Meisingset, O. Skogheim, B. Ekehov, and K. Wikstrøm, "Viklandet and Tunnsjødal SVCs - design, project execution and operating experience," in *Proceedings of CIGRÉ meeting 2010*, Paris, France, Aug.22-27 2010.

[34] M. Lahtinen, T. Rauhala, H. Kuisti, J. Peltola, and P. Halonen, "Static var compensator enhancing the operational reliability of Finnish transmission network," in *Proceedings of CIGRÉ meeting 2010*, Paris, France, Aug.22-27 2010.

[35] N. G. Hingorani and L. Gyugyi, *Understanding FACTS: Concepts and Technology of Flexible AC Transmission Systems*. IEEE press, 2000.

[36] R. Mathur and R. K. Varna, *Thyristor-based FACTS controllers for electrical transmission systems*. John Wiley & Sons–IEEE Press, 2002.

[37] IEEE Special Stability Controls Working Group, "Static var compensator models for power flow and dynamics performance simulation," *IEEE Transactions on Power Systems*, vol. Vol. 9, pp. 229–240, Feb. 1994.

[38] *PSS^{TM}E 31.0 Program Application Guide: Volume II*, Siemens Power Transmission & Distribution, Inc. - Power Technology International, Dec. 2007, www.siemens.com/power-technologies.

[39] P. Pourbeik, D. J. Sullivan, A. Boström, J. Sanchez-Gasca, Y. Kazachkov, J. Kowalski, A. Salazar, A. Meyer, R. Lau, D. Davies, and E. Allen, "Generic model structures for simulating static var systems in power system studies–A WECC task force effort," *IEEE Transactions on Power Systems*, vol. 27, no. 3, pp. 1618–1627, Aug. 2012.

[40] M.K. Jalboub, A.M. Ihbal, H.S. Rajamani, R.A. Abd-Alhameed, and A.M. Ihbal, "Determination of static voltage stability-margin of the power system prior to voltage collapse," in *2011 8th International Multi-Conference on Systems, Signals and Devices (SSD)*, Mar.22–25 2011, pp. 1–6.

[41] Nord Pool Spot, "Maximum net transfer capacity map," Oct. 2012. [Online]. Available: http://www.nordpoolspot.com/Global/Download%20Center/TSO/Max_NTC_20111010_valid-from-15-Dec.pdf

[42] J. Machowski, J. W. Bialek, and J. R. Bumby, *Power System Dynamics: Stability and Control*, 2nd ed. John Wiley & Sons, 2008.

[43] L. Lima and J. Feltes, "Pss®e test system for voltage collapse analysis," Siemens Energy, Inc., Siemens PTI eNewsletter 104, Jul. 2009.

[44] R. Grunbaum, P. Halvarsson, D. Larsson, and P. R. Jones, "Conditioning of power grids serving offshore wind farms based on asynchronous generators," in *Power Electronics, Machines and Drives, 2004. (PEMD 2004). Second International Conference on (Conf. Publ. No. 498)*, vol. 1, Mar.31–Apr.2 2004, pp. 34–39.

[45] B. Maya, S. Sreedharan, and J. G. Singh, "An integrated approach for the voltage stability enhancement of large wind integrated power systems," in *Power, Signals, Controls and Computation (EPSCICON), 2012 International Conference on*, Jan.3–6 2012, pp. 1–6.

[46] M. Narimani and R. K. Varma, "Application of Static Var Compensator (SVC) with fuzzy controller for grid integration of wind farm," in *Electrical and Computer Engineering (CCECE), 2010 23rd Canadian Conference on*, May2–5 2010, pp. 1–6.

[47] *PSS^{TM}E 31.0 Volume II: Program Operation Manual*, Siemens Power Transmission & Distribution, Inc. - Power Technology International, Dec. 2007, www.siemens.com/power-technologies.

[48] C. Rahmann, H.-J. Haubrich, A. Moser, R. Palma-Behnke, L. Vargas, and M. B. C. Salles, "Justified fault-ride-through requirements for wind turbines in power systems," *Power Systems, IEEE Transactions on*, vol. 26, no. 3, pp. 1555–1563, 2011.

[49] Y. Kazachkov and K. Patil, *PSS^{TM}E Model for GE-1.5/3.6 MW Wind Turbines*, Siemens Power Transmission & Distribution, Inc. - Power Technology International, Apr. 2008, www.siemens.com/power-technologies.

[50] *BID 2.4 Manual - Commissioned by SvK*, Pöyry.

[51] "Conversations with Hilda Dahlsten, power system analyst, Svenska Kraftnät, Sundbyberg," 2013.

[52] Álvaro José Pessoa Ramos and H. Tyll, "Dynamic performance of a radial weak power system with multiple static VAr compensators," *Power Systems, IEEE Transactions on*, vol. 4, no. 4, pp. 1316–1325, 1989.

[53] S. Choi, J. R. Stewart, B. Singh, P. F. Carrington, E. H. Goddard, and C. E. Carter, "Performance testing of a long distance radial static VAr compensated transmission system and validation of simulation results," *Power Systems, IEEE Transactions on*, vol. 3, no. 4, pp. 1509–1517, 1988.

www.kth.se